A new Holocene record of geomagnetic secular variation from Windermere, UK

Rachael S. Avery[a] (R.Avery@noc.soton.ac.uk; corresponding author)
Chuang Xuan[a] (C.Xuan@soton.ac.uk)
Alan E. S. Kemp[a] (aesk@noc.soton.ac.uk)
Jonathan M. Bull[a] (bull@noc.soton.ac.uk)
Carol J. Cotterill[b] (cjcott@bgs.ac.uk)
J. James Fielding[a] (jjf1e13@soton.ac.uk)
Richard B. Pearce[a] (r.pearce@noc.soton.ac.uk)
Ian W. Croudace[a] (iwc@noc.soton.ac.uk)

[a]University of Southampton, National Oceanography Centre, Southampton, Southampton, United Kingdom SO14 3ZH
[b]British Geological Survey, Lyell Centre, Research Avenue South, Edinburgh, United Kingdom EH14 4AP

Abstract

Paleomagnetic secular variation (PSV) records serve as valuable independent stratigraphic correlation and dating tools for marine and terrestrial sediment sequences, and enhance knowledge of geomagnetic field dynamics. We present a new radiocarbon-dated record (WINPSV-12K) of Holocene geomagnetic secular variation from Windermere, updating the existing 1981 UK master PSV curve. Our analyses used continuous U-channel samples taken from the center of four sediment cores retrieved from Windermere in 2012. The natural remanent magnetization (NRM) of each U-channel was measured before and after stepwise alternating field (AF) demagnetization on a superconducting rock magnetometer at intervals of 0.5-cm or 1-cm. The NRM data reveal a stable and well-defined primary magnetization.

Component declinations and inclinations estimated using Principal Component Analysis (PCA) of NRM data from the four Windermere cores correlate well on their independent radiocarbon age models. The four records were stacked using a sliding window bootstrap method, resulting in a composite Holocene PSV record (WINPSV-12K).

On millennial timescales WINPSV-12K correlates well with other records from Western Europe and the northern North Atlantic to a resolution of ~1 kyr, given age uncertainties and spatial variability between records. WINPSV-12K also compares well to the CALS10k.2 and pfm9k.1a model predictions for Windermere. Key regionally-significant PSV inclination features of WINPSV-12K which correlate with other North Atlantic records include peaks at 5 – 6, 8.5, and 10 cal ka BP, and a trough at 7 cal ka BP. Key PSV declination features include the eastward swing from 5.5 – 2.3 cal ka BP followed by a major westward excursion at 2.3 cal ka BP, peaks at 1.1 and 7cal ka BP, and troughs at 5.4 and 8.2 cal ka BP, with the caveat that an estimated magnetic lock-in delay of at least 100 – 200 years is present. PSV variations on 1 – 3 kyr timescales are interpreted to represent strengthening and weakening of the North American versus the Siberian and European-Mediterranean high-latitude flux lobes, based on the close similarities between the North Atlantic regional records and the antiphase existing in the East Asian Stack record and the North East Pacific inclination stack. WINPSV-12K provides a regionally-important new PSV reference curve whose prominent features may serve as stratigraphic markers for North Atlantic paleo-records.

Keywords

Paleomagnetism, Flux lobes, lake sediments, Holocene, Windermere, Paleosecular Variation

1. Introduction

Paleomagnetic secular variation (PSV) describes the variation in the Earth's geomagnetic field on timescales of a hundred years or longer in periods of stable magnetic polarity, and exhibits substantial variation throughout the Holocene (Turner et al., 2015; Turner and Thompson, 1981; Zheng et al., 2014). Fine magnetic particles in marine and lacustrine settings often preserve the direction and intensity information of the Earth's magnetic field during and shortly after deposition, forming a continuous PSV archive. Lake sediments are conducive to paleo-record preservation due to relatively high sedimentation rates, good accessibility, and little influence from currents, waves, and macrofaunal bioturbation. PSV records reconstructed from marine and lacustrine sediments have become increasingly utilized over the last few decades (Mackereth, 1971; Ojala and Saarinen, 2002; Snowball et al., 2007; Stoner et al., 2013, 2007; Turner et al., 2015; Zheng et al., 2014). These records provide continuous information on geomagnetic field dynamics beyond historical observations and archaeological measurements (Batt et al., 2017; Jackson et al., 2000), and provide data to inform and improve geomagnetic field models (Brown and Korte, 2016; Constable et al., 2016; Nilsson et al., 2014) while serving as a valuable stratigraphic correlation and dating tool that is independent of climate and ecological systems (Ólafsdóttir et al., 2013). In sediment cores exhibiting high sedimentation rates and little bioturbation, PSV records are particularly suitable for dating and improving the correlation of sedimentary records even over large regions (Zheng et al., 2014), and are thus valuable in developing understanding of rapid changes and diachroneity in the Earth System at high temporal resolution. There is a need across locations used in the study of late Quaternary climate variability to produce and utilize more PSV records using reliable dating methods, high measurement resolution (1 cm or better), and continuous sampling and measurement techniques. Having an independent dating and stratigraphic tool other than tephra layers enables the correlation of more spatially distributed records, especially between locations with no common tephra horizons.

The location of Windermere, UK, provides an opportunity to link continental Europe with Icelandic and Greenlandic records (Fig. 1). Measurement of declination in the UK demonstrated the potential for the use of PSV as a dating method (Mackereth, 1971). The UK PSV master curve constructed in 1979-81 (Thompson and Turner, 1979; Turner and Thompson, 1981) has been used both to date other PSV records from around Europe (Saarinen, 1999; Vigliotti, 2006) and also in the construction of several paleomagnetic field models, thus furthering understanding of the geomagnetic field (Constable et al., 2016). There has been little study of

UK-based Holocene paleomagnetic records since the development of the existing UK master curve, which was largely dated using 20 cm thick bulk radiocarbon samples using older radiocarbon processing methods (Thompson and Turner, 1979; Turner and Thompson, 1981). New piston cores from Windermere provide the opportunity to update the UK master curve (which was constructed partially from cores from Windermere, along with Llyn Geirionydd and Loch Lomond) using modern dating and paleomagnetic analyses. The new cores span the length of Windermere, whereas the Windermere cores collected by Turner using a 'Mackereth' corer were all from a location similar to that of our Core 57 (Fig. 1) (Turner and Thompson, 1981).

In this study, we construct a composite Holocene PSV record (WINPSV-12K) using four sediment cores from Windermere, UK (Fig. 1), with a view to updating the UK PSV master curve (Thompson and Turner, 1979; Turner and Thompson, 1981). The accelerator mass spectrometry (AMS) radiocarbon-dated record is high-resolution, with core sedimentation rates of 20 - 50 cm/kyr and paleomagnetic measurements every 0.5 – 1 cm. WINPSV-12K is compared to well-dated records from the North Atlantic (Mazaud et al., 2012; Stoner et al., 2013), Scandinavia (Sagnotti et al., 2012; Snowball et al., 2007), the existing UK master PSV curve (Turner and Thompson, 1981), the UK archeomagnetic curve (Batt et al., 2017), eastern Canada (Barletta et al., 2010), East Asia (Zheng et al., 2014), and the North East Pacific (Walczak et al., 2017). WINPSV-12K serves as a valuable new curve for synchronization of Holocene marine-terrestrial records across the northern North Atlantic (NNA) geomagnetic region.

2. Materials and Methods

2.1 Geological setting of Windermere

Windermere, situated in the southeast of the English Lake District near the West coast of England (54.04° N, 2.95° W), is a north-south trending glacial ribbon lake in a steep-sided pre-glacial river valley overdeepened by successive glaciations (Pennington and Pearsall, 1973; Pinson et al., 2013). The lake is 17 km long with a maximum width of 1.5 km, an elevation of 39 m above Ordnance Datum Newlyn, and a present maximum

water depth of 62 m (Lowag et al., 2012; Miller et al., 2013). Windermere drains a catchment of 242 km^2 (Miller et al., 2013) with Ordovician Borrowdale Volcanic Group bedrock in the north and Windermere Supergroup (Silurian mudstones and siltstones) in the south. A bedrock high separates Windermere into a north and south basin, and a sill dams the lake in the south forcing drainage to the west into the River Leven (Wilson, 1987). Windermere in its present form has been accumulating sediment since exposure following the retreat of the British-Irish Ice Sheet c. 17 ka BP (Ballantyne et al., 2009; Coope and Pennington, 1977).

2.2 Coring and core stratigraphy

A multibeam bathymetry site survey coupled with chirp, parametric, and multi-channel boomer seismic reflection surveys were used to identify sediment depocenters which had not been significantly disturbed by meter-scale mass transport deposits (Lowag et al., 2012; Miller et al., 2013; Vardy et al., 2010). Several sediment cores were collected using both a Uwitec piston corer and Uwitec gravity corer in 2012 as part of a coring campaign by the British Geological Survey (BGS) and the University of Southampton. Piston cores were acquired in 2 m sequential sections with 9 cm diameter core barrels. The piston core sections were then cut into 1 m sections and split lengthways into working and archive halves. Four 6 - 10 m long cores with the highest deposition rates and longest timespans of the core suite were selected for this study (Fig. 2).

Each of the four cores has an inorganic mineral-rich base and a brown organic-rich top with a sharp transition between the two major lithologies (Fig. 2). Cores from the North Basin (Cores 64 and 68) have disturbed bases attributed to oscillating proximal glaciers in the north basin catchment, whilst the bases of the cores from the south basin (Cores 57 and 67) have thick cm-scale varves comprising silt and clay. Overlying the basal sediment of all four cores are mm-scale clastic silt and clay varves. These are overlain by an organic-bearing non-varved silty clay unit with differing small-scale features in each core (e.g. diatoms, iron inclusions, presence/absence of laminations) controlled by depocenter-specific conditions. This is succeeded by a unit of mm-scale clastic varves, overlain in turn by a relatively uniform, organic-rich, intermittently-laminated brown pelletized mud of Holocene age. Mass-transport deposits (MTDs) are present in all cores, mostly of a thickness less than 20 cm, although there are two thicker MTDs: one in the Lateglacial sediment of the South Basin (1.5

m), and the other in the early Holocene sediment of the North Basin (0.53 m) (Fig. 2). Inspection of the microstructure of the sediment using a scanning electron microscope and transmitted light microscope indicate that MTDs are not present in the Holocene sediment of the piston cores except at the base.

2.3 Paleomagnetic samples and measurements

The four cores were continuously sampled using U-channels (~1.8 × 1.9 cm^2 cross-section and the length of the core section) from the center of the working half of each core section. The natural remanent magnetization (NRM) of each U-channel was measured at the University of Southampton on a 2G Enterprises superconducting rock magnetometer (SRM) designed for U-channel samples. Measurements for each U-channel were made at 0.5-cm (Core 68) or 1-cm (Cores 57, 64, and 67, since the results were equally good but quicker to produce) intervals with an additional 10 cm measured beyond both ends of the sample. NRM of the U-channels were measured before and after stepwise alternating field (AF) demagnetization with peak fields up to 100 mT (see Supplementary Table 1 for details). After completion of NRM measurements for each U-channel, an anhysteretic remanent magnetization (ARM) was imparted in a 100-mT peak AF and a 50-μT direct current (DC) bias field along the long-axis of the U-channel. The acquired ARM was measured prior to demagnetization and after stepwise AF demagnetization at the same peak fields used for NRM. Subsequently, the U-channels were used for progressive ARM acquisition, during which each U-channel acquired increasing ARM as the peak AF (along the long axis of the U-channel) was increased using the same peak fields used for NRM with a constant 50-μT DC bias field. For each ARM acquisition step, the acquired (partial) ARM was measured at the same intervals as for NRM.

Bulk sediment samples from representative lithologies of the four cores were taken for room temperature hysteresis loops, backfield, and isothermal remanent magnetization (IRM) acquisition experiments on a Princeton Measurements Corp. Model 3900 Vibrating Sample Magnetometer (VSM) at the University of Southampton. IRM of the samples were acquired and measured at fifty field steps on a logarithmic scale ranging from ~0.4 μT to 1 T. Hysteresis loops of the samples were measured at 5-mT field steps, with the applied field ranging between -1 T and +1 T. For the backfield experiment, a 1-T field was first applied,

followed by repeated remanence measurements after increasing the applied field (with a 2-mT increment) in the opposite direction until zero remanence was reached. Hysteresis loop data were drift-corrected following the procedures suggested by Jackson and Solheid (2010), and normalized against sample mass. Selected bulk samples were also freeze-dried and ground, then magnetic susceptibility of the samples was monitored on heating from room temperature to 700 °C and subsequent cooling to room temperature, in an argon gas environment, using an AGICO KLY-4S Susceptibility Bridge.

2.4 Age model construction

Age models for Cores 57, 67, 64 and 68 (Fig. 3) were constructed using 4, 6, 4, and 9 accelerator mass spectrometry (AMS) radiocarbon dates respectively. Dates were ascertained from both macrofossils such as terrestrial leaves and twigs, and from 1 cm thickness bulk sediment samples. Radiocarbon sample depths are indicated in Fig. 2. Radiocarbon dates were provided by the NERC Radiocarbon Facility in East Kilbride, Scotland, and dates were calibrated using Calib 7.1 (Stuiver and Reimer, 1993) and the Intcal13 calibration curve (Reimer et al., 2013). An additional date at each core top was acquired using ^{137}Cs and ^{210}Pb radiochronology. Dating sample details are summarized in Supplementary Table 2.

Sections of sediment containing MTDs were removed from the depth records prior to construction of a 'normal sedimentation' age model (Fig. 3). The start of the Holocene has been dated to ~11.7 cal ka BP (Walker et al., 2009), and the radiocarbon dates from the Windermere cores show that an abrupt lithological transition from inorganic-dominant silt and clay varves to organic-rich intermittently laminated mud occurred around this time. We therefore take this transition to mark the start of the Holocene in Windermere.

3. Results

3.1 Magnetic minerology

Median destruction field (MDF) of the NRM across the four cores (Supplementary Fig. 1a - d) ranges from 44-58 mT (comparable to 43-45 mT reported by Turner and Thompson (1981) for Windermere cores). NRM of the Holocene sediment in all four cores was completely demagnetized after AF demagnetization with a 100 mT peak field (see Fig. 4), suggesting a low-coercivity Holocene NRM carrier such as magnetite. Magnetic susceptibility of Holocene samples from the cores show a possible Hopkinson peak at ~520 °C upon heating (Fig. 5a) and abrupt decrease or increase at temperatures of ~580-585 °C during heating (Fig. 5a) and cooling (Fig. 5b) respectively, further suggesting magnetite as the primary magnetization carrier in the Holocene sediment. Additionally, gradients of the IRM acquisition curves for Holocene sediments follow normal distributions (on logarithmic field scales) with mean coercivity of ~50-70 mT (Fig. 5c - d), consistent with magnetite being the primary remanence carrier. Hysteresis loop data (Fig. 5e) show that the Holocene sediment samples typically reach saturation at an applied field of <100 mT, and contain a significant amount of paramagnetic materials. Coercivity of remanence for the samples is mostly around 45 mT (inlet in Fig. 5e). Hysteresis parameter ratios (i.e. Mr/Ms and Hcr/Hc, where Mr, Ms, Hcr, and Hc are saturation remanence, saturation magnetization, coercivity of remanence, and coercivity, respectively) of all Holocene samples are shown on a Day et al. (1977) plot in Fig. 5f. Holocene sediments from all four cores fall into the pseudo-single domain (PSD) category, in the area associated with fine magnetite particles.

AF demagnetization on NRM of pre-Holocene (Lateglacial) sediments in the cores clearly show the presence of a high coercivity component (e.g. Supplementary Fig. 2). Further magnetic mineralogy experiments including hysteresis loops and IRM acquisition also indicate the existence of a high coercivity magnetic mineral. This high coercivity magnetic component clearly has a large influence on NRM of the sediments, for example large inclination deviations of tens of degrees from the Holocene interval and from the expected geocentric axial dipole (GAD) inclination for the core locations. It is possible that magnetite in the Holocene Windermere sediments is soil-derived through soil magnetite enrichment (Mullins, 1977), while Lateglacial Windermere sediments are mainly derived from erosion of the up-catchment weathered volcanic bedrock that could contain hematite (Stone et al., 2010). The pre-Holocene Windermere sediments are not considered suitable for PSV studies due to large lithology-induced inclination fluctuations. This PSV study therefore focuses on Windermere's Holocene sediments, with magnetite as the single primary magnetization carrier.

The Holocene sediments of Windermere appear similar between cores, and relatively uniform within-core (with the exception of the very early Holocene, where terrigenous material is more abundant). The base sediment matrix comprises pelletized mud containing organic fragments and numerous microfossils (e.g. diatoms and chironomids), with no detectable carbonate. Each core exhibits intermittent millimeter-scale laminations which differ in detrital versus organic material, and therefore density. Some iron variations correspond with these laminations, which can vary over several laminae. The bands are much thinner than the SRM response function and upon inspection of the sediment do not appear to affect the downcore magnetic parameters. The mineralogy experiments also confirm that fine-grained magnetite is dominant throughout the Holocene. Total organic content for the majority of the Holocene is typically 9-15%. Downcore values of ARM/κ (where κ is magnetic susceptibility) for Cores 67, 64, and 68 largely follow the general pattern of ARM, whilst ARM/κ for Core 57 is in antiphase with NRM MDF (Supplementary Fig. 1).

3.2 Paleomagnetic directional records

For each U-channel measurement interval, component magnetization directions were calculated using principal component analysis (PCA, Kirschvink, 1980) and UPmag software (Xuan and Channell, 2009). PCA calculations used NRM data acquired during the 20-60 mT demagnetization interval (without anchoring directions to the origin of orthogonal projections), and are associated with maximum angular deviation (MAD) values that monitor the quality of fitting for the PCA. MAD values associated with the PCA estimates for all four cores are generally <1°, indicating the component directions are very well defined (see Supplementary Fig. 1a - d). Results were removed from intervals with voids, apparent disturbance (including the core tops), and MTDs. Results from the top and bottom 4 cm of the U-channels were also removed to avoid edge effects due to convolution of the magnetometer sensor response function.

The studied cores had not been azimuthally oriented during coring and splitting, so declination values for each core-section are arbitrary. The approximate time duration covered by individual 1 m core sections ranges from approximately 1 – 4 kyr according to the radiocarbon based age models. Correction of declination values of each core by a simple subtraction of the mean was considered unsuitable because significant secular variation

occurs on this millennial timescale. Component declinations of each core were placed on their independent radiocarbon age models and compared to the well-dated Greenland-Iceland composite declination record (Stoner et al., 2013, 2007). Declination correction for each core section was performed by subtracting the mean difference between prominent declination features on the Greenland-Iceland composite curve and those of each Windermere core section where they overlap in time. Cores used to construct the Greenland-Iceland composite curve had been split on a constant plane (Stoner et al., 2007) and declination of the cores had been corrected to have zero mean, which is reasonable considering that over ten thousand years of geomagnetic behavior is being averaged (Merrill and McFadden, 2003).

Component inclinations from the four cores vary between 54° to 83° with similar mean values of ~65 - 70°. On the radiocarbon chronology, component inclinations of the cores show correlations. The age model for each core was refined by transferring selected radiocarbon dates (closed square; Fig. 6) from the other three cores through correlating appropriate inclination features. The refined age models (dashed lines; Fig. 3) were then used for other down-core records. On a millennial timescale, component inclinations from the four cores show a similar pattern including steeper inclinations between 1 - 7 cal ka BP and shallower inclinations between 6 - 9 cal ka BP (Figs. 6 and 7a). Common sub-millennial inclination features include the four peaks between ~3.5 - 6 cal ka BP and similar variabilities between ~8.5 - 11.5 cal ka BP. Corrected declinations from the four cores also show common features such as high-amplitude variabilities since 4 cal ka BP and relatively low amplitude changes prior to 4 cal ka BP (Fig. 7b). There are also differences in both inclination and declination records between the four cores, especially on centennial timescales. These differences could be caused by changes in sedimentation rates not accounted for by the radiocarbon dates from each core (Ólafsdóttir et al., 2013), the differing smoothing effects of the sediment magnetization process (due to lock-in) from each sedimentation rate, and age model uncertainties. The cores may also have subtly-differing lithologies, since they are situated in separate sediment depocenters (Fig. 1). Differences between the paleomagnetic directions of the four cores do not appear to relate to higher MAD values. ARM/k and NRM MDF both show similar overall trends: ARM/ κ in all four cores indicates magnetic grain size slightly fining upward from the base of the Holocene to about 6 cal ka BP, then slightly coarsening throughout the remainder

of the Holocene (and the Day Plot also shows little difference in grain size within and between cores), so magnetic grain size does not appear to underlie the between-core differences.

To average out noise and highlight common paleomagnetic directional changes, the direction and intensity records of the Windermere cores were stacked over the last ~12 kyr to form WINPSV-12K. Construction of the stack records followed a similar method to Xuan et al. (2016) for a North Atlantic paleointensity stack (HINAPIS) record. The four Holocene records were normalized to have common means and standard deviations for each variable. The stacking was performed at 50-year intervals between -50 and 11750 cal y BP, with an interval half-window size of 150 years (comparable to the mean uncertainty of the calibrated ages). At each interval center and for each variable, 2500 values were randomly taken from each core record within the interval window. A square interval window was used, giving all age possibilities within the window an equal weight. Each subsequent window overlapped with the previous one by 250 y. For each time interval, the stack was formed from the mean of the total randomly taken values (10,000 where no core records had gaps), and the top and bottom 5% of values were identified to estimate the 90% confidence intervals (Fig. 7).

3.3 Relative paleointensity estimates

Normalized records of sedimentary NRM are often used as a proxy for relative paleointensity (RPI) of the geomagnetic field (Levi and Banerjee, 1976; Tauxe, 1993). Normalization is generally carried out using laboratory-induced magnetization such as anhysteretic remanent magnetization (ARM), isothermal remanent magnetization (IRM), or magnetic susceptibility, to compensate for changes in magnetic concentration of remanence carrying grains. For each 0.5-cm (Core 68) or 1-cm (Cores 57, 67, and 64) measurement interval of the Windermere cores, RPI proxies (Supplementary Fig. 1) were calculated using the slopes of best-fit lines between NRM lost vs. ARM lost as well as NRM lost vs. ARM acquired during 20-60 mT treatment steps (where the slopes of best-fit lines between NRM lost and ARM acquired are multiplied by -1). RPI estimates were determined using the UPmag software (Xuan and Channell, 2009), and each slope calculation was accompanied by a linear correlation coefficient (R-value) that monitors the quality of the line fit (mean R-values sat around 0.981 – 0.996).

4. Discussion

4.1 Holocene PSV at Windermere

The WINPSV-12K inclination stack (Fig. 7a) exhibits centennial-scale variation with peak-to-trough boundaries of 55° - 75° and a mean of ~65°, close to (and slightly shallower than) the expected geocentric dipole inclination of ~70° at Windermere. The whole Holocene inclination stack shows a quasi-regular inclination variability on a ~1-kyr timescale, with each swing (peak to trough) being ~6°. WINPSV-12K inclinations are generally shallower between 6 - 12 cal ka BP (mean of ~63°) and steeper since 6 cal ka BP (mean of ~69°). Notable inclination stack features include characteristic peaks at ~8.5 and ~11 cal ka BP, and troughs at ~7 and ~10 cal ka BP.

The WINPSV-12K declination stack exhibits peak-to-trough variation within a range of 55° (Fig. 7b). The individual declination curves follow similar trends on a multi-kyr timescale but are less similar on short timescale than the inclination curves, possibly related to uncertainties on core section declination corrections. An eastward declination feature from ~2.5 - 3.5 cal ka BP dominates the record, accompanied by other prominent eastward declinations at ~1, ~4.7, and ~7 cal ka BP. WINPSV-12K declination also exhibits marked troughs (i.e. westward declinations) at ~2.2, ~5.4, and ~8.2 cal ka BP.

The four RPI records generally agree with each other on millennial timescales, showing high RPI between ~3 - 5 cal ka BP, and low RPI between ~6 - 11 cal ka BP and after ~2.5 cal ka BP (Fig. 7c). On sub-millennial timescales, the four records correlate are less well. A reliable RPI record would not correlate with the normalizer, since a high correlation implies inappropriate normalization and undue influence of grain size or lithology on the RPI signal. RPI estimates from Cores 57, 67, and 68 show low correlations with their corresponding normalizer records (Supplementary Figs. 1 and 3), suggesting the RPI records from these cores

are generally not influenced by lithology. The strong correlation between RPI and ARM for core 64 is mostly caused by the sediment younger than 2.5 cal ka BP (~0.8 m depth) (Supplementary Figs. 1c and 3c).

The RPI stack exhibits a broadly similar trend on a multi-millennial timescale to other published records from nearby regions, including FENNORPIS (Snowball et al., 2007), the stacked EGLACOM and SVAIS records from the Barents Sea (Sagnotti et al., 2012), and IODP Site U1305 (Stoner et al., 2013) (Fig. 8). The Barents Sea, FENNORPIS, and Windermere records all show generally decreasing RPI from early Holocene to ~7 cal ka BP. After ~7 cal ka BP, the Barents Sea, FENNORPIS, and IODP Site U1305 records show increasing RPI until ~1-3 cal ka BP, followed by decreasing RPI. The Windermere RPI, however, starts to decline after ~3.8 cal ka BP in all four cores (Fig. 7c). No apparent changes in lithology or magnetic remanence carrier were observed over the last ~4 kyr, compared with the earlier Holocene sediment. The disparity of the Windermere RPI compared with other records during the last 3.8 kyr is likely related to inappropriate normalization (probably over-normalization) of the NRM in the upper sediments. For example, subtle changes in floc size due to changes in lake-wide water chemistry (e.g. salinity) around 3.8 cal ka BP could have led to changes in NRM acquisition efficiency (e.g. Tauxe et al., 2006) that are not accounted for by the ARM record. However, we currently cannot rule out that the drop-off in RPI starting ~3.8 cal ka BP could represent a genuine difference in field behavior at Windermere compared with the other locations (Fig. 1).

4.2 Comparison with records from other locations

In Figs. 9 and 10, the WINPSV-12K inclination and declination stack records are compared with other well-dated records from nearby locations and from farther afield (Fig. 1). Comparison curves include the North-East Pacific Inclination Anomaly Stack (NEPSIAS; Walczak et al., 2017), the East Asia Stack (Zheng et al., 2014), the Barents Sea record (Sagnotti et al., 2012), FENNOSTACK (Snowball et al., 2007), the existing UK master curve (Turner and Thompson, 1981) and the archeomagnetic curve from the British Isles (Batt et al., 2017), the Iceland-Greenland composite record (Stoner et al., 2013, 2007), the IODP Site U1305 record (Stoner et al., 2013), and the Eastern Canadian Stack (Barletta et al., 2010).

WINPSV-12K shares most of its inclination and declination features with the existing UK master curve (Figs. 9 and 10), which incorporates data from Loch Lomond, Lake Geirionydd, and Windermere. WINPSV-12K has an inclination peak between 5.3 – 6 cal ka BP not present in the UK master but prominent in the IODP Site U1305, Greenland-Iceland, and FENNOSTACK records. Similarly, WINPSV-12K has a small double-peak in declination at ~4.7 and ~5.9 cal ka BP which is present in the Greenland-Iceland stack and IODP Site U1305 but not present in the UK master. The 50-year time increment and 150-year averaging half-window used during the stacking produces a smoother record than the existing UK master curve, with reduced noise associated with centennial inclination features.

Over the whole Holocene, WINPSV-12K shows similar inclination behavior to other regional (i.e. North Atlantic margin) records, i.e. a gradual steepening in inclination through the Holocene, and particularly since 7 cal ka BP. The opposite trend is apparent in the Eastern Canadian stack, possibly implying weakening in the North American flux lobe and strengthening in the European flux lobe (Stoner et al., 2013). On multimillennial timescales (i.e. 2 – 3 kyr), WINPSV-12K shows similar features to other regional records. For the inclination records, this includes the inclination peaks centered at 8.5 and 11 cal ka BP, a trough centered at 7 cal ka BP, and a peak at 5.3 – 5.9 cal ka BP. These features may be used as key regional stratigraphic markers. In the declination records, the main regional feature is the apparent gradual eastward swing starting from ~5.4 cal ka BP, followed by a major westward excursion at ~2 – 2.3 cal ka BP. This feature is so prominent it can be correlated over a long distance: the same feature is seen in the East Asia stack but in antiphase. There exist other similarly well-correlated declination features, notably characteristic peaks at ~7 and 1.1 cal ka BP, and troughs at 9.3 and 5.4 cal ka BP.

On a centennial scale, the WINPSV-12K directional features appear slightly older (0 – 3 centuries) than those of IODP Site U1305, Iceland-Greenland composite records, and FENNOSTACK. When the age uncertainty envelope (Fig. 7) is considered, the only one of these records which differs significantly from Windermere (i.e. age differences consistently greater than the averaging window) is FENNOSTACK.

There are several possible reasons for the observed age differences of declination and inclination (and RPI prior to ~4 cal ka BP) features among the records. Snowball et al. (2007) note that the existing UK master curve is consistently older than FENNOSTACK by a few centuries and attribute this to dating problems in the UK master curve, where almost every date was ascertained using bulk sediment samples ~20 cm thick. The dating used in the current study, however, is higher quality than that of the existing UK master curve, with the use of ^{210}Pb and ^{37}Cs radiochronology for the core tops, AMS radiocarbon dating, a higher proportion of radiocarbon samples being macrofossils, and any bulk samples being only 1 cm thick rather than ~20 cm. Most of the macrofossils used are terrestrial (e.g. leaves and twigs), precluding radiocarbon hard-water error in at least these samples; furthermore Windermere is not a hard-water catchment. It is therefore unlikely that excessive dating uncertainty is the cause for the observed age differences. Bioturbation has also been suggested as a cause for greater ages for PSV records of the UK master curve (Snowball et al., 2007), but microscopic analysis of the sediment shows little evidence for the bioturbation mixed layer being greater than 1cm (~20 – 50 yr) .

There is likely a delay in magnetization "lock-in" in the Windermere sediments. The depth at which the Windermere sediment becomes cohesive enough to piston-core is ~19-25 cm, which corresponds to an age of ~90-140 years (based on ^{210}Pb and ^{37}Cs dates in the gravity and piston cores). This possible lock-in time is comparable to those reported for other European lake sediments (Haltia-Hovi et al., 2010; Saarinen, 1999; Snowball and Sandgren, 2002; Zolitschka et al., 2000), and may partly explain the observed age differences (up to 300 yr for FENNOSTACK, and up to 150 yr for other records). When compared with the archeomagnetic record (Batt et al., 2017) and the ARCH3K.1 model predictions (Korte et al., 2009), the WINPSV-12K declination matches well, and appears around 80 years older than the archeomagnetic curves. The inclination records match less well between 2.5 – 1.5 cal ka BP and after 0.8 cal ka BP. Where the records match, the apparent age difference is somewhat greater, around 150 years. Compaction in the tops of the cores during coring may have influenced inclination values in the last thousand years. Overall it is likely that the time lag caused by lock-in for the upper part of the Windermere record is between 100 - 200 years. Downcore, the sedimentation rate decreases such that in the period between 7.4 – 9.6 cal ka BP, the sedimentation rate of all four cores drops to below 20 cm/kyr. Lock-in caused time delay increases with decreasing sedimentation

417 rate, explaining why certain features of WINPSV-12K, especially between 7.4 – 9.6 cal ka BP, have a greater
418 age offset than those up-core. It should be noted that for the existing UK master curve, Llyn Geirionydd and
419 Loch Lomond are both reported to have higher sedimentation rates than Windermere (Turner and Thompson,
420 1981) partially explaining why it appears a little younger than WINPSV-12K in places (although the difference
421 is likely mostly due to differing dating methods).
422
423 The observed age differences in directional features on WINPSV-12K (and possibly the UK master) and
424 FENNOSTACK could also be caused by geomagnetic field spatial variability. Higher between-record
425 variability is expected between spatially-distributed records where geomagnetic structure is more prevalent.
426 Windermere's inclination and declination curves appear to share more similarity with those of the Iceland-
427 Greenland composite record and IODP Site U1305 than FENNOSTACK or the Barents Sea (Figs. 9 and 10),
428 despite U1305 being twice the distance from Windermere longitudinally than the FENNOSTACK records'
429 location (Fig. 1).
430
431
432 *4.3 Comparison with model predictions*
433
434 WINPSV-12K was compared against the CALS10k.2 and the pfm9k.1a model predictions for Windermere
435 (Constable et al., 2016; Nilsson et al., 2014). CALS10k.2 is a time varying spherical harmonic model of the
436 geomagnetic field over the last 10 kyr, based on both archeomagnetic and sediment-based geomagnetic data.
437 The pfm9k.1a model is also a spherical harmonic model and uses the same data as CALS10k.2, but treats the
438 data differently (e.g. changing the weight distribution of sedimentary archives and adding more weight to
439 archaeological sources). The pfm9k.1a model prediction was acquired from the GEOMAGIA database (Brown
440 et al., 2015).
441
442 Both models incorporate data from the original UK master curve. The two model predications of PSV at
443 Windermere are very similar to one another, the main difference being the amplitude of the inclination peak
444 at 5.3 – 5.9 cal ka BP (pfm9k.1a has the higher amplitude). The model predictions are rather similar to the

Greenland-Iceland inclination curve before 5 cal ka BP, meaning the pattern in WINPSV-12K between 5 - 7 cal ka BP is replicated in the models but that the inclination peak at 8.5 cal ka BP appears older than the model predictions (the data contributing to the Greenland-Iceland stack are included in the models (Korte et al., 2011; Stoner et al., 2007). After 5 cal ka BP, both models show more similarity to the UK master curve, meaning some centennial-scale features do not quite correlate with WINPSV-12K, likely because of dating differences. However, the millennial-scale features are shared between data and models (e.g. the inclination peaks at ~1.5, ~2.5, and 4.4 cal ka BP). The declination model curves have reduced amplitude compared with the WINPSV-12K data (and also the UK master curve data). The timing of features in the models is close to that of the Greenland-Iceland declination data, so the WINPSV-12K declination curve can lag the model by 100 – 400 yr in places (e.g. ~7, ~4.5, and 1 cal ka BP). This difference is likely related to magnetization lock-in (especially around 7 cal ka BP), which is minimal in the Greenland-Iceland stack due to its very high sedimentation rate (Stoner et al., 2013), but is estimated to be 100-200 years in the latter-Holocene Windermere sediment and possibly longer in the earlier Holocene (section 4.2). The only major difference between WINPSV-12K and the models is in the inclination record between 7 and 9.7 cal ka BP. The main peak of the inclination feature lags the model by ~300 yr, but also the steepness of the inclination drops before that of the models and some other records. In addition to lag caused by lock-in, the fact that two of the individual Windermere cores (i.e. Cores 64 and 67) have core section breaks around this interval have likely contributed to the lower inclination values of WINPSV-12K (Fig. 7a).

4.4 Implications on geomagnetic field behavior

Historical geomagnetic field measurements clearly show persistent regions of concentrated geomagnetic flux (i.e. flux lobes) at the core-mantle boundary, which may reflect long-term regulation of heat flux from the core to the mantle (e.g. Bloxham and Gubbins, 1985; Jackson et al., 2000). Through comparisons of well-dated high-resolution Holocene PSV records from the northern North Atlantic (NNA) and Eastern Canada (North America), Stoner et al. (2013) hypothesized that Holocene PSV is largely driven by oscillations of flux concentrations at a few recurrent high-latitude locations (e.g. below Canada, Siberia, and the Europe/Mediterranean region). The authors recognized two distinct modes controlling the PSV records: a

"North American mode" characterised by high North American intensities, western North Atlantic declination, and GAD-like virtual geomagnetic poles (VGPs); and a "European mode" characterised by relatively low North American intensities, eastward North Atlantic declination, and lower latitude VGPs. Walczak et al. (2017) recently constructed a NE Pacific sedimentary inclination anomaly stack (NEPSIAS) capturing the common signal over an area spanning over 30° longitude and latitude from Alaska through Oregon to Hawaii (Fig. 1a). NEPSIAS inclinations largely co-vary with NNA declinations during the Holocene (i.e. steeper NE Pacific inclinations are associated with westward NNA declinations), suggesting that the Pacific is sensitive to temporal variability in the relative strength of distal flux-lobe features in quasi-persistent locations under North America and Europe (Walczak et al., 2017).

Similar to PSV records from the NNA, WINPSV-12K declinations and inclinations are more consistent with European than North American records (Figs. 9 and 10). The East Asia inclination stack shows a broadly in-phase relationship to the NEPSIAS and an apparently anti-phase relationship to the NNA and European records on 1-3 kyr timescales. The fact that a relationship exists among these PSV records spanning such a large area (20-70° in latitudes and almost all longitudes; Figure 1a), suggests that PSV from these regions are responding to a common forcing at this timescale. The East Asian Stack and NEPSIAS (perhaps also East Canadian Stack for some time intervals) are in antiphase with the NNA and European records for most of the Holocene, implying that the activity of the competing flux lobes is occurring between the sites of the East Asia stack/NEPSIAS and the NNA and European regional records. For example, the eastward swing in declination between 5.4 and 2.3 cal ka BP in the NNA and European records, and the westward swing in the East Asia Stack along with the shallowing of inclination in the NEPSIAS and Eastern Canadian Stack suggest a steady weakening of the North American flux lobe while the Siberian and European/Mediterranean region flux lobes strengthen. The VGP positions estimated from the WINPSV-12K, the East Asia, and the Barents Sea PSV records all show an apparent trend approximately along the 45°E-135°W longitude line (Supplementary Fig. 4). The offset between the different VGP position estimates could be related to declination correction and resolution of the individual records. The ~45°E-135°W longitude line may represent the main axis between the competing flux lobes, linking the "North American mode" and "European/Mediterranean mode".

5. Conclusions

Paleomagnetic inclination and declination records from the Windermere cores show similar features on millennial timescale and were stacked to create a new PSV reference curve for the UK, WINPSV-12K. WINPSV-12K inclination and declination compare well with the CALS10k.2 and pfm9k.1a model predictions for Windermere on millennial timescales. Comparison of WINPSV-12K directional records with other PSV curves from the NNA- Europe region demonstrates that there are inclination and declination features on the millennial scale which may be confidently correlated and could act as partial isochrones, especially when inclination or declination features are well-constrained by tephra dating or reliable radiocarbon dates across multiple records. Dating uncertainties and noise in both the Windermere and the other presented records make correlation on timescales shorter than a few centuries difficult. Over the whole Holocene, WINPSV-12K shows similar behavior to other regional records, especially on timescales of 2 – 3 kyr. For inclination, this includes the wide peaks at 8.5 cal ka BP and 10 cal ka BP, a trough at 7 cal ka BP, and a peak at 5-6 cal ka BP. The most prominent declination feature is the apparent eastward motion starting from ~5.5 cal ka BP, followed by a major westward excursion at ~2 – 2.3 cal ka BP. These regionally-significant features may be used as key stratigraphic markers, with the caveat that in the latter half of the Holocene a magnetic lock-in delay of 100 – 200 years is estimated, and that due to reduced sedimentation rates in the early Holocene (prior to 7.4 cal ka BP), the lock-in delay here is likely to be greater.

The antiphase relationship between the NNA regional records and NEPSIAS and the East Asia Stack on 1 – 3 kyr timescales indicates that competition between high-latitude flux lobes is a common driver for PSV variations throughout the Northern Hemisphere on these timescales, and that the main axis for competition between flux lobes could be the ~45°E - 135°W longitude line.

WINPSV-12K represents an update to the existing UK master curve. Given the location of the UK between continental European archives and records from Iceland and Greenland, a fully-updated UK PSV master curve for the Holocene is of great importance to correlations between these regions.

Acknowledgements

We are grateful to Richard and Daniel Niederreiter, Helen Miller, John Davis, and Stuart Jarvis for their support during sediment coring, and to the BGS marine operations crew and hydrographic surveyors of the R/V White Ribbon. We thank Martin Dodgson and the Windermere Lake Wardens for their assistance, as well as the Freshwater Biological Association.

We are very grateful to Martin Frank and two anonymous reviewers for their helpful comments, which greatly improved this manuscript.

Charlotte Bryant advised on radiocarbon dating. This work was supported by the NERC Radiocarbon Facility NRCF010001 (allocation numbers 1746.1013 and 1856.1014), the BGS University Funding Initiative (Reference S243), and the University of Southampton.

Carol J Cotterill publishes with the permission of the Executive Director of the British Geological Survey, Natural Environment Research Council.

References

Ballantyne, C.K., Stone, J.O., Fifield, L.K., 2009. Glaciation and deglaciation of the SW Lake District, England: implications of cosmogenic 36Cl exposure dating. Proc. Geol. Assoc. 120, 139–144. doi:10.1016/j.pgeola.2009.08.003

Barletta, F., St-Onge, G., Stoner, J.S., Lajeunesse, P., Locat, J., 2010. A high-resolution Holocene paleomagnetic secular variation and relative paleointensity stack from eastern Canada. Earth Planet. Sci. Lett. 298, 162–174. doi:10.1016/j.epsl.2010.07.038

Batt, C.M., Brown, M.C., Clelland, S.-J., Korte, M., Linford, P., Outram, Z., 2017. Advances in archaeomagnetic dating in Britain: New data, new approaches and a new calibration curve. J. Archaeol. Sci. 85, 66–82. doi:10.1016/j.jas.2017.07.002

Bloxham, J., Gubbins, D., 1985. The secular variation of Earth's magnetic field. Nature 317, 777–779.

Brown, M.C., Donadini, F., Korte, M., Nilsson, A., Korhonen, K., Lodge, A., Lengyel, S.N., Constable, C.G., 2015. GEOMAGIA50.v3: 1. general structure and modifications to the archeological and volcanic

database, Earth, Planets and Space. doi:10.1186/s40623-015-0232-0

Brown, M.C., Korte, M., 2016. A simple model for geomagnetic field excursions and inferences for palaeomagnetic observations. Phys. Earth Planet. Inter. 254, 1–11. doi:10.1016/j.pepi.2016.03.003

Constable, C., Korte, M., Panovska, S., 2016. Persistent high paleosecular variation activity in southern hemisphere for at least 10000 years. Earth Planet. Sci. Lett. 453, 78–86. doi:10.1016/j.epsl.2016.08.015

Coope, G.R., Pennington, W., 1977. The Windermere Interstadial of the late Devensian. Philos. Trans. R. Soc. London. B 280, 337–339.

Day, R., Fuller, M., Schmidt, V.A., 1977. Hysteresis properties of titanomagnetites: grain-size and compositional dependence. Phys. Earth Planet. Inter. 13, 260–267.

Haltia-Hovi, E., Nowaczyk, N., Saarinen, T., 2010. Holocene palaeomagnetic secular variation recorded in multiple lake sediment cores from eastern Finland. Geophys. J. Int. 180, 609–622. doi:10.1111/j.1365-246X.2009.04456.x

Jackson, A., Jonkers, R.T., Walker, M.R., 2000. Four centuries of geomagnetic secular variation from historical records. Phil. Trans. R. Soc. Lond. A 358, 957–990. doi:10.1029/2002RG000115

Jackson, M., Solheid, P., 2010. On the quantitative analysis and evaluation of magnetic hysteresis data. Geochemistry, Geophys. Geosystems 11, 1–25. doi:10.1029/2009GC002932

Kirschvink, J.L., 1980. The least-squares line and plane and the analysis of paleomagnetic data. Geophys. J. R. Astron. Soc. 62, 699–718. doi:10.1111/j.1365-246X.1980.tb02601.x

Korte, M., Constable, C., Donadini, F., Holme, R., 2011. Reconstructing the Holocene geomagnetic field. Earth Planet. Sci. Lett. 312, 497–505. doi:10.1016/j.epsl.2011.10.031

Korte, M., Donadini, F., Constable, C.G., 2009. Geomagnetic field for 0-3 ka: 2. A new series of time-varying global models. Geochemistry, Geophys. Geosystems 10. doi:10.1029/2008GC002297

Levi, S., Banerjee, S.K., 1976. On the possibility of obtaining relative paleointensities from lake sediments. Earth Planet. Sci. Lett. 29, 219–226. doi:10.1016/0012-821X(76)90042-X

Lowag, J., Bull, J.M., Vardy, M.E., Miller, H., Pinson, L.J.W., 2012. High-resolution seismic imaging of a

Younger Dryas and Holocene mass movement complex in glacial lake Windermere, UK. Geomorphology 171–172, 42–57. doi:10.1016/j.geomorph.2012.05.002

Mackereth, F.J.H., 1971. On the variation in direction of the horizontal component of remanent magnetisation in lake sediments. Earth Planet. Sci. Lett. 12, 332–338. doi:10.1016/0012-821X(71)90219-6

Mazaud, A., Channell, J.E.T., Stoner, J.S., 2012. Relative paleointensity and environmental magnetism since 1.2Ma at IODP site U1305 (Eirik Drift, NW Atlantic). Earth Planet. Sci. Lett. 357–358, 137–144. doi:10.1016/j.epsl.2012.09.037

Merrill, R.T., McFadden, P.L., 2003. The geomagnetic axial dipole field assumption. Phys. Earth Planet. Inter. 139, 171–185. doi:10.1016/j.pepi.2003.07.016

Miller, H., Bull, J.M., Cotterill, C.J., Dix, J.K., Winfield, I.J., Kemp, A.E.S., Pearce, R.B., 2013. Lake bed geomorphology and sedimentary processes in glacial lake Windermere, UK. J. Maps 1–14. doi:10.1080/17445647.2013.780986

Mullins, C.E., 1977. Magnetic Susceptibility of the Soil and Its Significance in Soil Science - a Review. J. Soil Sci. 28, 223–246. doi:10.1111/j.1365-2389.1977.tb02232.x

Nilsson, a., Holme, R., Korte, M., Suttie, N., Hill, M., 2014. Reconstructing Holocene geomagnetic field variation: new methods, models and implications. Geophys. J. Int. 198, 229–248. doi:10.1093/gji/ggu120

Ojala, A.E.K., Saarinen, T., 2002. Palaeosecular variation of the Earth's magnetic field during the last 10000 years based on the annually laminated sediment of Lake Nautajärvi, central Finland. The Holocene 12, 391–400. doi:10.1191/0959683602hl551rp

Ólafsdóttir, S., Geirsdóttir, Á., Miller, G.H., Stoner, J.S., Channell, J.E.T., 2013. Synchronizing holocene lacustrine and marine sediment records using paleomagnetic secular variation. Geology 41, 535–538. doi:10.1130/G33946.1

Pennington, W., Pearsall, W.H., 1973. Glaciation-the shaping of the landscape, in: The Lake District: A Landscape History. Collins: London.

Pinson, L.J.W., Vardy, M.E., Dix, J.K., Henstock, T.J., Bull, J.M., Maclachlan, S.E., 2013. Deglacial history

606 of glacial lake windermere, UK: implications for the central British and Irish Ice Sheet. J. Quat. Sci. 28,
607 83–94. doi:10.1002/jqs.2595

608 Reimer, P., Bard, E., Bayliss, A., Beck, J.W., Blackwell, P.G., Buck, C.B.R.C.E., Cheng, H., Edwards, R.L.,
609 Friedrich, M., Grootes, P.M., Guilderson, T.P., Haflidason, H., Hajdas, I., Hatté, C., Heaton, T.J.,
610 Hoffmann, D.L., Hogg, A.G., Hughen, K.A., Kaiser, K.F., Kromer, B., Manning, S.W., Niu, M., Reimer,
611 R.W., Richards, D.A., Scott, E.M., Southon, J.R., Staff, R.A., Turney, C.S.M., Plicht, J. van der, 2013.
612 IntCal13 and Marine13 Radiocarbon Age Calibration Curves 0–50,000 Years cal BP. Radiocarbon 55,
613 1869–1887. doi:10.2458/azu_js_rc.55.16947

614 Saarinen, T., 1999. Palaeomagnetic dating of late Holocene sediments in Fennoscandia. Quat. Sci. Rev. 18,
615 889–897. doi:10.1016/S0277-3791(99)00003-7

616 Sagnotti, L., MacRì, P., Lucchi, R., Rebesco, M., Camerlenghi, A., 2012. A Holocene paleosecular variation
617 record from the northwestern Barents Sea continental margin. Geochemistry, Geophys. Geosystems 12,
618 1–24. doi:10.1029/2011GC003810

619 Snowball, I., Sandgren, P., 2002. Geomagnetic field variations in northern Sweden during the Holocene
620 quantified from varved lake sediments and their implications for cosmogenic nuclide production rates.
621 The Holocene 12, 517–530. doi:10.1191/0959683602hl562rp

622 Snowball, I., Zillén, L., Ojala, A., Saarinen, T., Sandgren, P., 2007. FENNOSTACK and FENNORPIS: Varve
623 dated Holocene palaeomagnetic secular variation and relative palaeointensity stacks for Fennoscandia.
624 Earth Planet. Sci. Lett. 255, 106–116. doi:10.1016/j.epsl.2006.12.009

625 Stone, P., Millward, D., Young, B., Merritt, J.W., Clarke, S.M., McCormac, M., Lawrence, D.J.D., 2010.
626 Mineralization in the Lake District, in: British Regional Geology: Northern England. British Geological
627 Survey, Keyworth, Nottingham.

628 Stoner, J.S., Channell, J.E.T., Mazaud, A., Strano, S.E., Xuan, C., 2013. The influence of high-latitude flux
629 lobes on the Holocene paleomagnetic record of IODP Site U1305 and the northern North Atlantic.
630 Geochemistry, Geophys. Geosystems 14, 4623–4646. doi:10.1002/ggge.20272

631 Stoner, J.S., Jennings, A., Kristjánsdóttir, G.B., Dunhill, G., Andrews, J.T., Hardardóttir, J., 2007. A

paleomagnetic approach toward refining Holocene radiocarbon-based chronologies: Paleoceanographic records from the north Iceland (MD99-2269) and east Greenland (MD99-2322) margins. Paleoceanography 22, n/a-n/a. doi:10.1029/2006PA001285

Stuiver, M., Reimer, P.J., 1993. Extended 14C data base and revised CALIB 3.0 14C age calibration program. Radiocarbon 35, 215–230.

Tauxe, L., 1993. Sedimentary records of relative paleointenstiy of the geomagnetic field: theory and practice. Rev. Geophys. 31, 319–354.

Tauxe, L., Steindorf, J.L., Harris, A., 2006. Depositional remanent magnetization: Toward an improved theoretical and experimental foundation. Earth Planet. Sci. Lett. 244, 515–529. doi:10.1016/j.epsl.2006.02.003

Thompson, R., Turner, G., 1979. British geomagnetic master curve 10,000-0 yr BP for dating European sediments. Geophys. Res. Lett. 6, 249–252.

Turner, G.M., Howarth, J.D., de Gelder, G.I.N.O., Fitzsimons, S.J., 2015. A new high-resolution record of Holocene geomagnetic secular variation from New Zealand. Earth Planet. Sci. Lett. 430, 296–307. doi:10.1016/j.epsl.2015.08.021

Turner, G.M., Thompson, R., 1981. Lake sediment record of the geomagnetic secular variation in Britain during Holocene times. Geophys. J. Int. 65, 703–725. doi:10.1111/j.1365-246X.1981.tb04879.x

Vardy, M.E., Pinson, L.J.W., Bull, J.M., Dix, J.K., Henstock, T.J., Davis, J.W., Gutowski, M., 2010. 3D seismic imaging of buried Younger Dryas mass movement flows: Lake Windermere, UK. Geomorphology 118, 176–187. doi:10.1016/j.geomorph.2009.12.017

Vigliotti, L., 2006. Secular variation record of the Earth's magnetic field in Italy during the Holocene: Constraints for the construction of a master curve. Geophys. J. Int. 165, 414–429. doi:10.1111/j.1365-246X.2005.02785.x

Walczak, M.H., Stoner, J.S., Mix, A.C., Jaeger, J., Rosen, G.P., Channell, J.E.T., Heslop, D., Xuan, C., 2017. A 17,000 yr paleomagnetic secular variation record from the southeast Alaskan margin: Regional and global correlations. Earth Planet. Sci. Lett. 473, 177–189. doi:10.1016/j.epsl.2017.05.022

Walker, M., Johnsen, S., Rasmussen, S.O., Popp, T., Steffensen, J.-P., Gibbard, P., Hoek, W., Lowe, J., Andrews, J., Bjorck, S., Cwynar, L.C., Hughen, K., Kershaw, P., Kromer, B., Litt, T., Lowe, D.J., Nakagawa, T., Newnham, R., Schwander, J., 2009. Formal definition and dating of the GSSP (Global Stratotype Section and Point) for the base of the Holocene using the Greenland NGRIP ice core, and selected auxiliary records. J. Quat. Sci. 24, 3–17. doi:10.1002/jqs.1227

Wilson, C., 1987. The outflow of Windermere, Cumbria : a re-appraisal. Geol. J. 22, 219–224.

Xuan, C., Channell, J.E.T., 2009. UPmag: MATLAB software for viewing and processing u channel or other pass-through paleomagnetic data. Geochemistry, Geophys. Geosystems 10, 1–12. doi:10.1029/2009GC002584

Xuan, C., Channell, J.E.T., Hodell, D.A., 2016. Quaternary magnetic and oxygen isotope stratigraphy in diatom-rich sediments of the southern Gardar Drift (IODP Site U1304, North Atlantic). Quat. Sci. Rev. 142, 74–89. doi:10.1016/j.quascirev.2016.04.010

Zheng, Y., Zheng, H., Deng, C., Liu, Q., 2014. Holocene paleomagnetic secular variation from East China Sea and a PSV stack of East Asia. Phys. Earth Planet. Inter. 236, 69–78. doi:10.1016/j.pepi.2014.07.001

Zolitschka, B., Brauer, a., Negendank, J.F.W., Stockhausen, H., Lang, a., 2000. Annually dated late Weichselian continental paleoclimate record from the Eifel, Germany. Geology 28, 783–786. doi:10.1130/0091-7613(2000)28<783:ADLWCP>2.0.CO

Fig. Captions

Fig. 1. Above: Map of the 10 – 90° N latitudes, showing the locations of both Windermere (red star) and comparative records (other markers). Right: Map of the catchment of Windermere with 100 m contour lines, multibeam lake bathymetry, and core locations. Inset: Location of Windermere in the British Isles (black box).

Fig. 2. Core image (left) and lithostratigraphy (right) of Windermere Cores 57, 67, 64, and 68. The Holocene PSV record is based on the dark brown organic sections of the four cores. Lithostratigraphic tie-points between the cores are included. Sediment ages given are median-probability radiocarbon dates in cal y BP calculated with Calib 7.1 (Stuiver and Reimer, 1993) using the Intcal13 calibration curve (Reimer et al., 2013).

Fig. 3. Age-depth profiles (upper panel) and sedimentation rates (lower panel) for Windermere Cores 57 (green), 67 (blue), 64 (red), and 68 (gray). Ages are based on calibrated (Calib7.1; Stuiver and Reimer, 1993) radiocarbon dates (NRCF 1736.1013; NRCF 1856.1014) calibrated with the IntCal13 calibration curve (Reimer et al., 2013). Markers indicate median probability calibrated radiocarbon dates, and error bars indicate the upper and lower 2σ age calibrations. Points are fitted using a linear interpolation. Smaller markers and dotted lines indicate transferred radiocarbon tie-points from other cores and thus the refined age model used when building the WINPSV-12K stack. Sedimentation rates are shown below on both original and refined age models.

Fig. 4. Representative NRM AF demagnetization behaviors of Holocene sediments of Cores 57, 67, 64, and 68. For each selected 1-cm interval from the four cores, the NRM intensity versus AF demagnetization step plot are shown on the left and the orthogonal projection plot of NRM is shown on the right (blue squares = horizontal projections, red circles = vertical projections). Three examples are shown from each core.

Fig. 5. Magnetic susceptibility of Holocene bulk sediments from the four cores monitored while (a) heating the samples from room temperature to 700°C, and (b) cooling the samples from 700°C to room temperature. (c) IRM acquisition curves for selected bulk samples from the four cores, (d) gradient of the IRM acquisition

curves, (e) hysteresis loops and backfield data of representative Holocene samples from the four cores, and (f) hysteresis parameter ratios of all measured Holocene samples shown on a Day et al. (1977) plot. The thermomagnetic curves show abrupt changes at ~580°C, and the gradient of IRM acquisition curves show single magnetic components with mean coercivity of ~50-70 mT.

Fig. 6. Holocene inclination curves for the Windermere suite (Core 57: green, Core 67: blue, Core 64: red, Core 68: gray) on refined age models, showing the locations of radiocarbon dates for each core (black squares) and radiocarbon dates transferred from other Windermere cores based on inclination features (black circles). Gray dashed lines indicate tiepoints between curves. Declination and RPI curves were subsequently placed on this age model (see Fig. 7).

Fig. 7. Stacked Windermere paleomagnetic records for (a) inclination; (b) declination; and (c) RPI. Each panel individual records from Cores 68 (gray), 64 (red), 67 (blue), and 57 (green) overlain with the WINPSV-12K stack (black) with 90% confidence interval estimate from 10,000 bootstrapped populations (gray envelope). Dipole inclination value for the latitude of Windermere is shown as dashed black line in Fig. 7(a). Key features of WINPSV-12K are marked with vertical arrows.

Fig. 8. WINPSV-12K RPI record compared with RPI records from nearby regions. From top to bottom: the Barents Sea (Sagnotti et al., 2012), FENNORPIS (Snowball et al., 2007), WINPSV-12K, and IODP U1305 (Mazaud et al., 2012).

Fig. 9. Comparison of WINPSV-12K inclination record with published records from the North Atlantic, Northern Europe, and East Asia. In order from the top: NEPSIAS (Walczak et al., 2017), East Asian Stack (Zheng et al., 2014), the Barents Sea (Sagnotti et al., 2012), FENNOSTACK (Snowball et al., 2007), the UK master curve (Turner and Thompson, 1981), WINPSV-12K, the Greenland-Iceland shallow marine composite (Stoner et al., 2013), IODP U1305 (Mazaud et al., 2012), and the Eastern Canadian Stack (Barletta et al., 2010). WINPSV-12K is shown overlain on the UK archeomagnetic curve (Batt et al., 2017; pale gray solid line), the ARCH3k.1 model (Korte et al., 2009; pale gray dotted line), the CALS10k.2 model (Constable et al.,

2016; dark gray dashed line), and the pfm9k.1a model (Nilsson et al., 2014; dark gray dotted line). Key inclination features of WINPSV-12K are shown with vertical black arrows.

Fig. 10. Comparison of WINPSV-12K declination record with published records from the North Atlantic, Northern Europe, and East Asia. In order from the top: NEPSIAS (Walczak et al ., 2017), East Asian Stack (Zheng et al., 2014), the Barents Sea (Sagnotti et al., 2012), FENNOSTACK (Snowball et al., 2007), the UK master curve (Turner and Thompson, 1981), WINPSV-12K, the Greenland-Iceland shallow marine composite (Stoner et al., 2013), IODP U1305 (Mazaud et al., 2012), and the Eastern Canadian Stack (Barletta et al., 2010). WINPSV-12K is shown overlain on the UK archeomagnetic curve (Batt et al., 2017; pale gray solid line), the ARCH3k.1 model (Korte et al., 2009; pale gray dotted line), the CALS10k.2 model (Constable et al., 2016; dark gray dashed line), and the pfm9k.1a model (Nilsson et al., 2014; dark gray dotted line). Key inclination features of WINPSV-12K are shown with vertical black arrows.

751

752 **Figures**

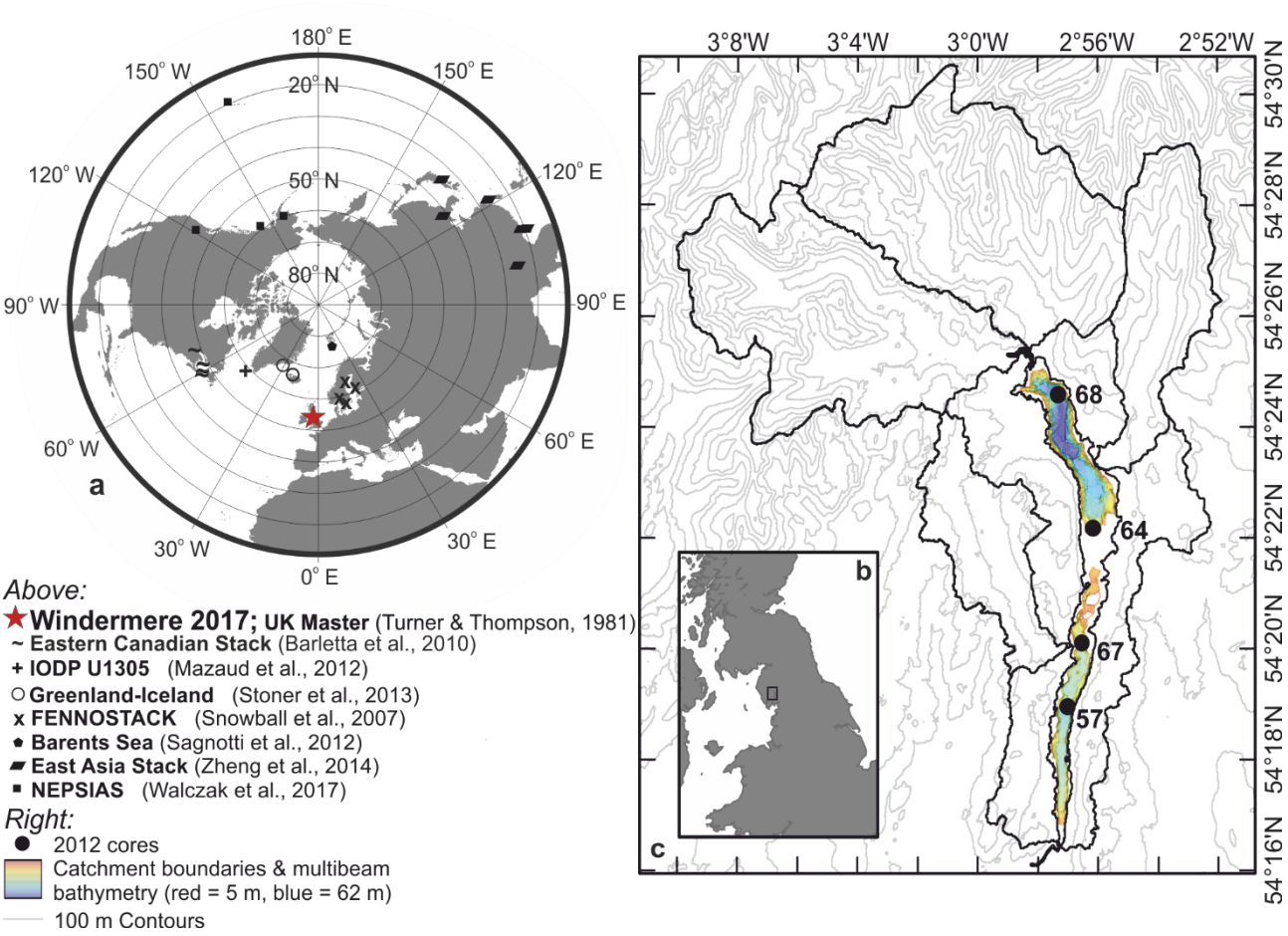

753

754

755 **Fig. 1**

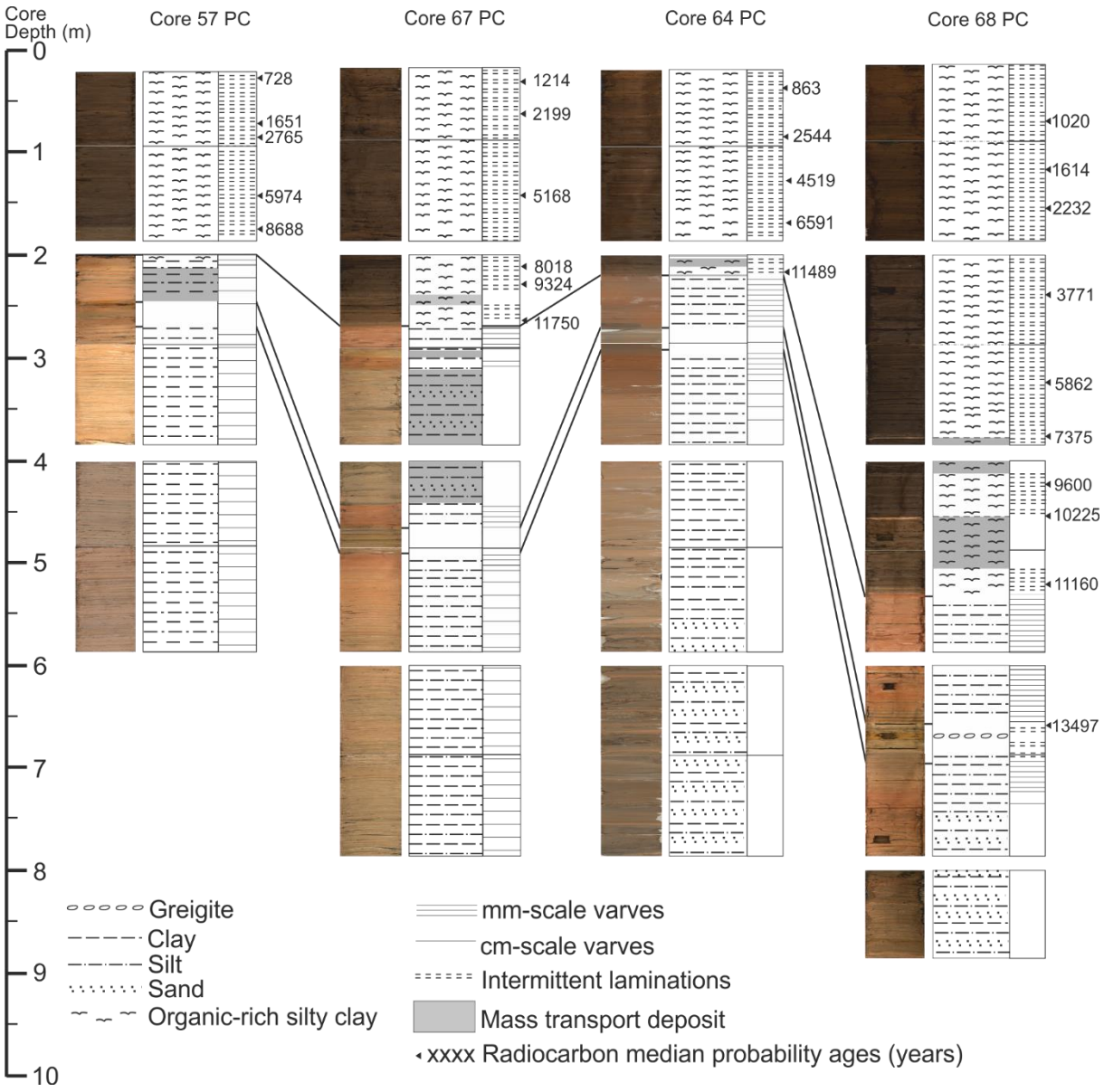
Core Depth (m)
Core 57 PC
Core 67 PC
Core 64 PC
Core 68 PC
0
1
2
3
4
5
6
7
8
9
10
728
1651
2765
5974
8688
1214
2199
5168
8018
9324
11750
863
2544
4519
6591
11489
1020
1614
2232
3771
5862
7375
9600
10225
11160
13497
Greigite
Clay
Silt
Sand
Organic-rich silty clay
mm-scale varves
cm-scale varves
Intermittent laminations
Mass transport deposit
xxxx Radiocarbon median probability ages (years)

Fig. 2

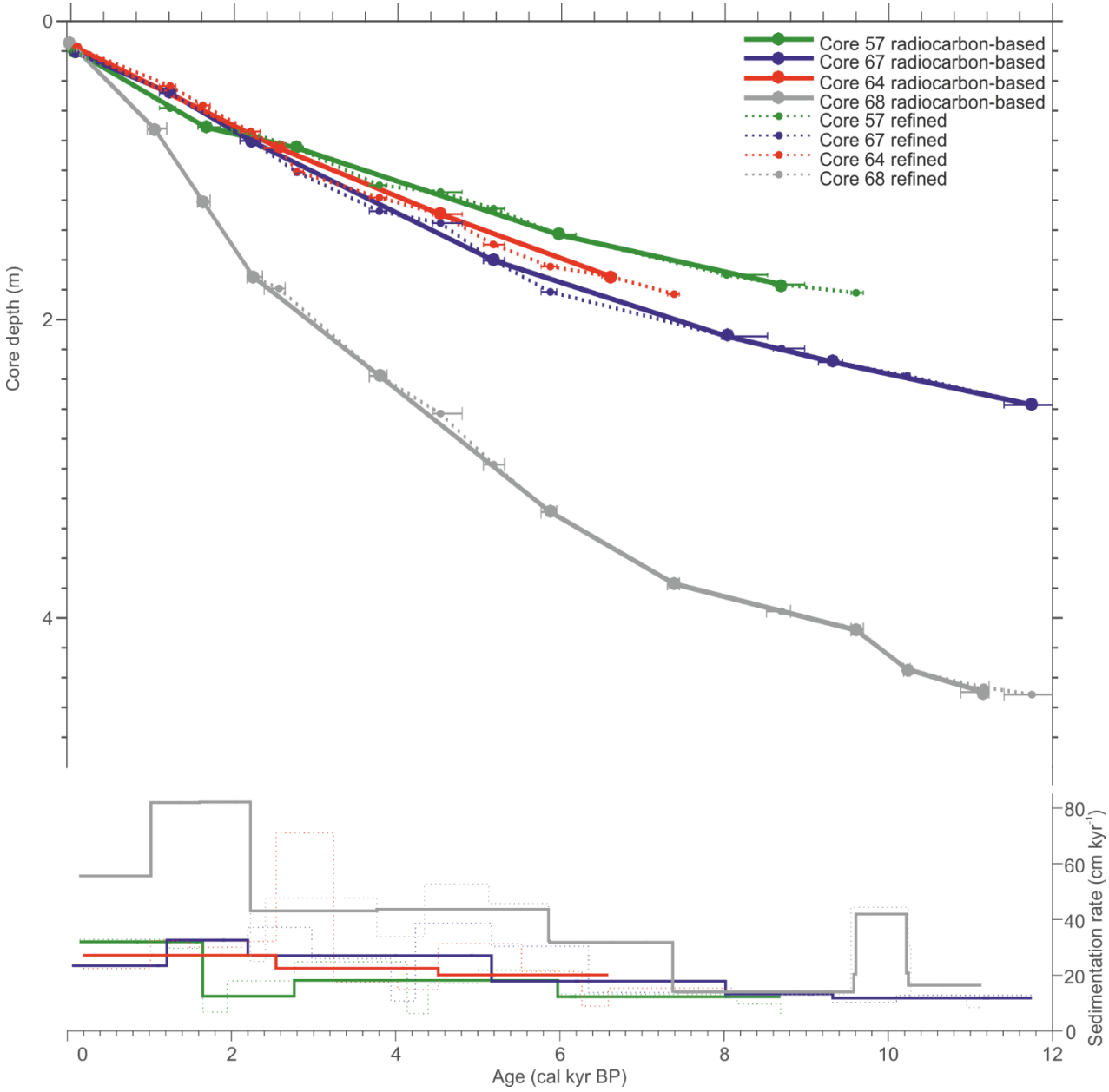
Core 57 radiocarbon-based
Core 67 radiocarbon-based
Core 64 radiocarbon-based
Core 68 radiocarbon-based
Core 57 refined
Core 67 refined
Core 64 refined
Core 68 refined
Core depth (m)
0
2
4
Age (cal kyr BP)
0
2
4
6
8
10
12
Sedimentation rate (cm kyr-1)
0
20
40
60
80

759

760 **Fig. 3**

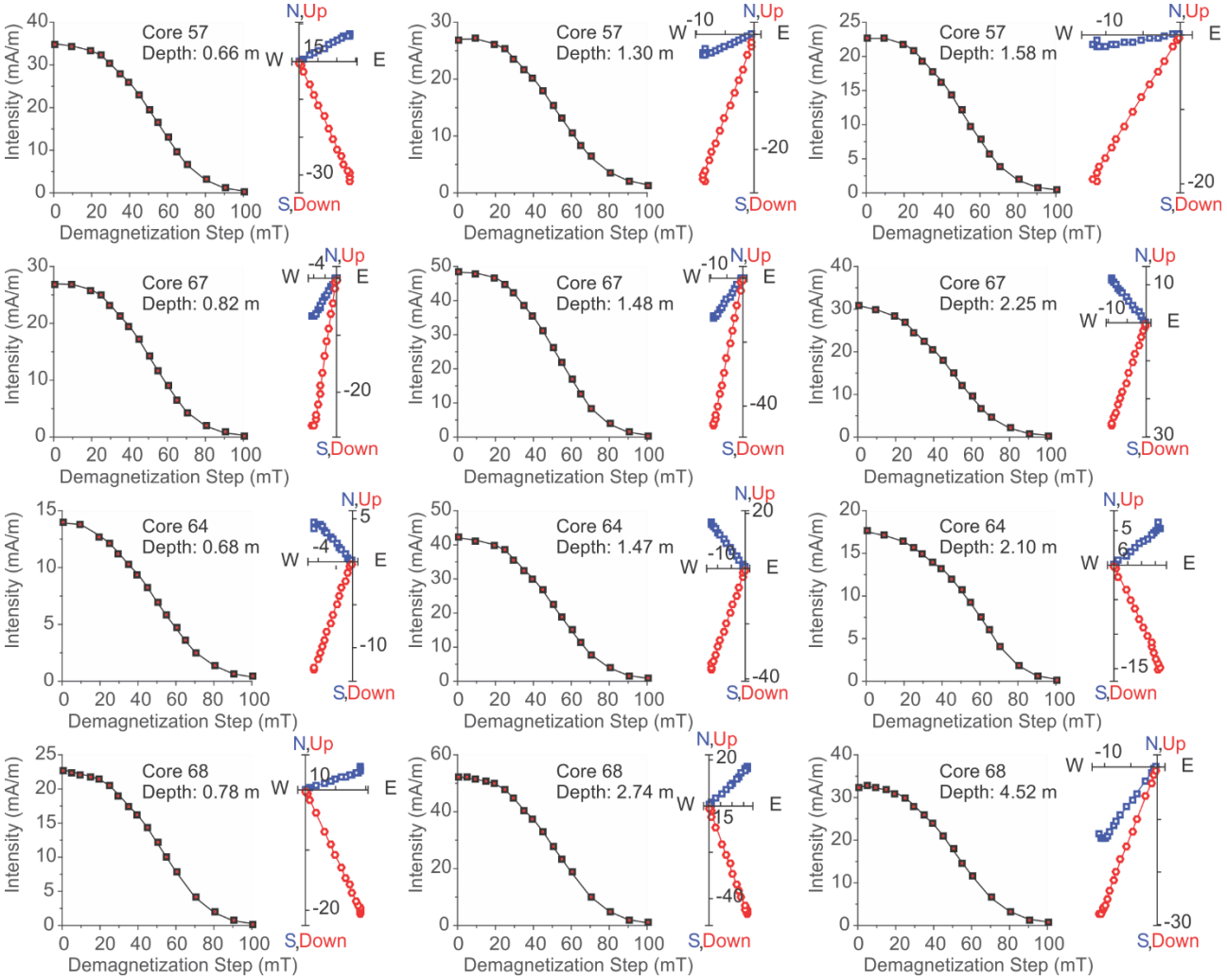
Core 57
Depth: 0.66 m
Core 57
Depth: 1.30 m
Core 57
Depth: 1.58 m
Core 67
Depth: 0.82 m
Core 67
Depth: 1.48 m
Core 67
Depth: 2.25 m
Core 64
Depth: 0.68 m
Core 64
Depth: 1.47 m
Core 64
Depth: 2.10 m
Core 68
Depth: 0.78 m
Core 68
Depth: 2.74 m
Core 68
Depth: 4.52 m
Intensity (mA/m)
Demagnetization Step (mT)
N,Up
S,Down
W
E

761

762 **Fig. 4**

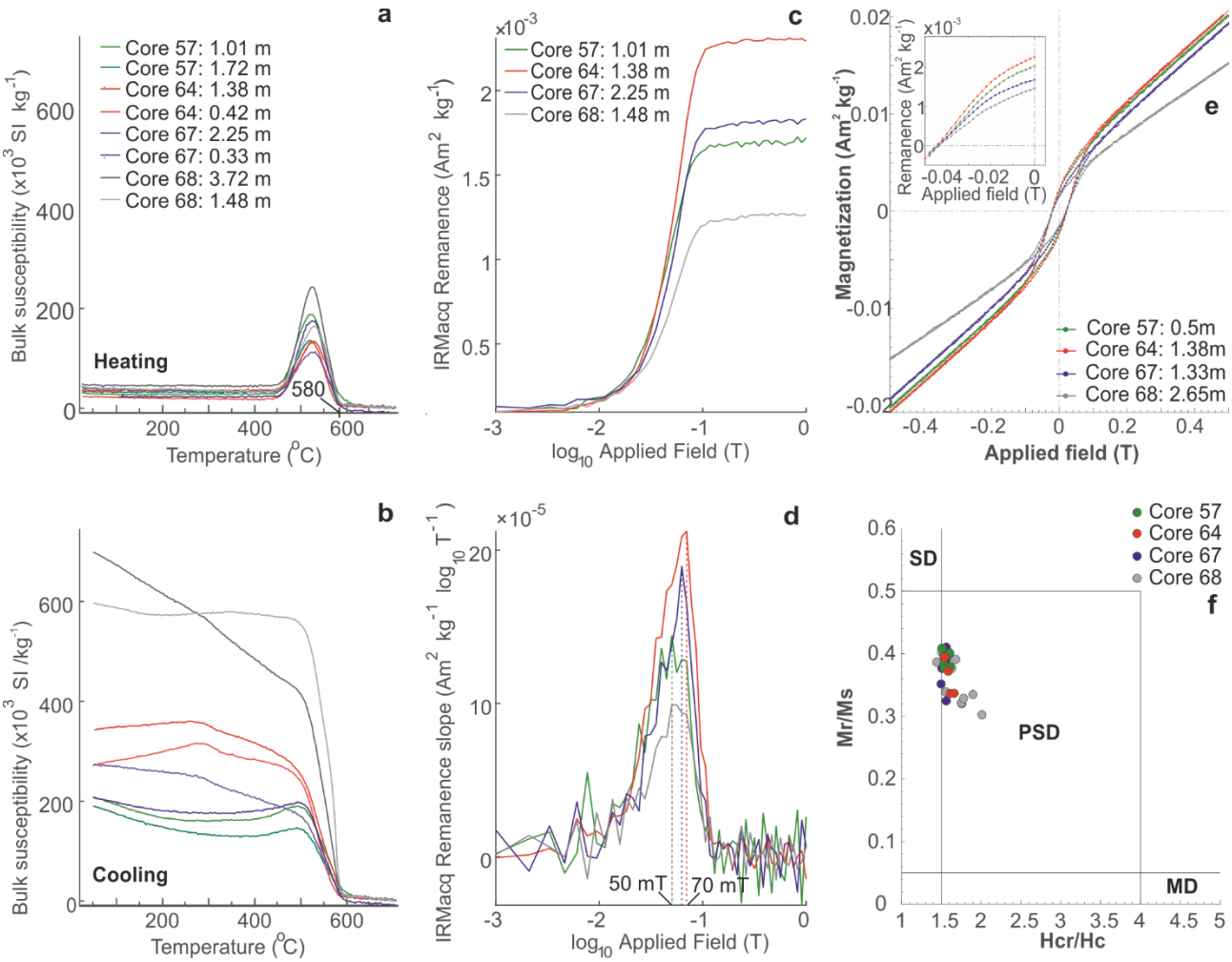
a
Core 57: 1.01 m
Core 57: 1.72 m
Core 64: 1.38 m
Core 64: 0.42 m
Core 67: 2.25 m
Core 67: 0.33 m
Core 68: 3.72 m
Core 68: 1.48 m
Bulk susceptibility (x10^3 SI kg^-1)
Heating
580
Temperature (°C)
b
Bulk susceptibility (x10^3 SI /kg^-1)
Cooling
Temperature (°C)
c
×10^-3
Core 57: 1.01 m
Core 64: 1.38 m
Core 67: 2.25 m
Core 68: 1.48 m
IRMacq Remanence (Am^2 kg^-1)
log10 Applied Field (T)
d
×10^-5
IRMacq Remanence slope (Am^2 kg^-1 log10 T^-1)
50 mT
70 mT
log10 Applied Field (T)
e
Remanence (Am^2 kg^-1)
×10^-3
Applied field (T)
Magnetization (Am^2 kg^-1)
Core 57: 0.5m
Core 64: 1.38m
Core 67: 1.33m
Core 68: 2.65m
Applied field (T)
f
Core 57
Core 64
Core 67
Core 68
SD
PSD
MD
Mr/Ms
Hcr/Hc

Fig. 5

765 —

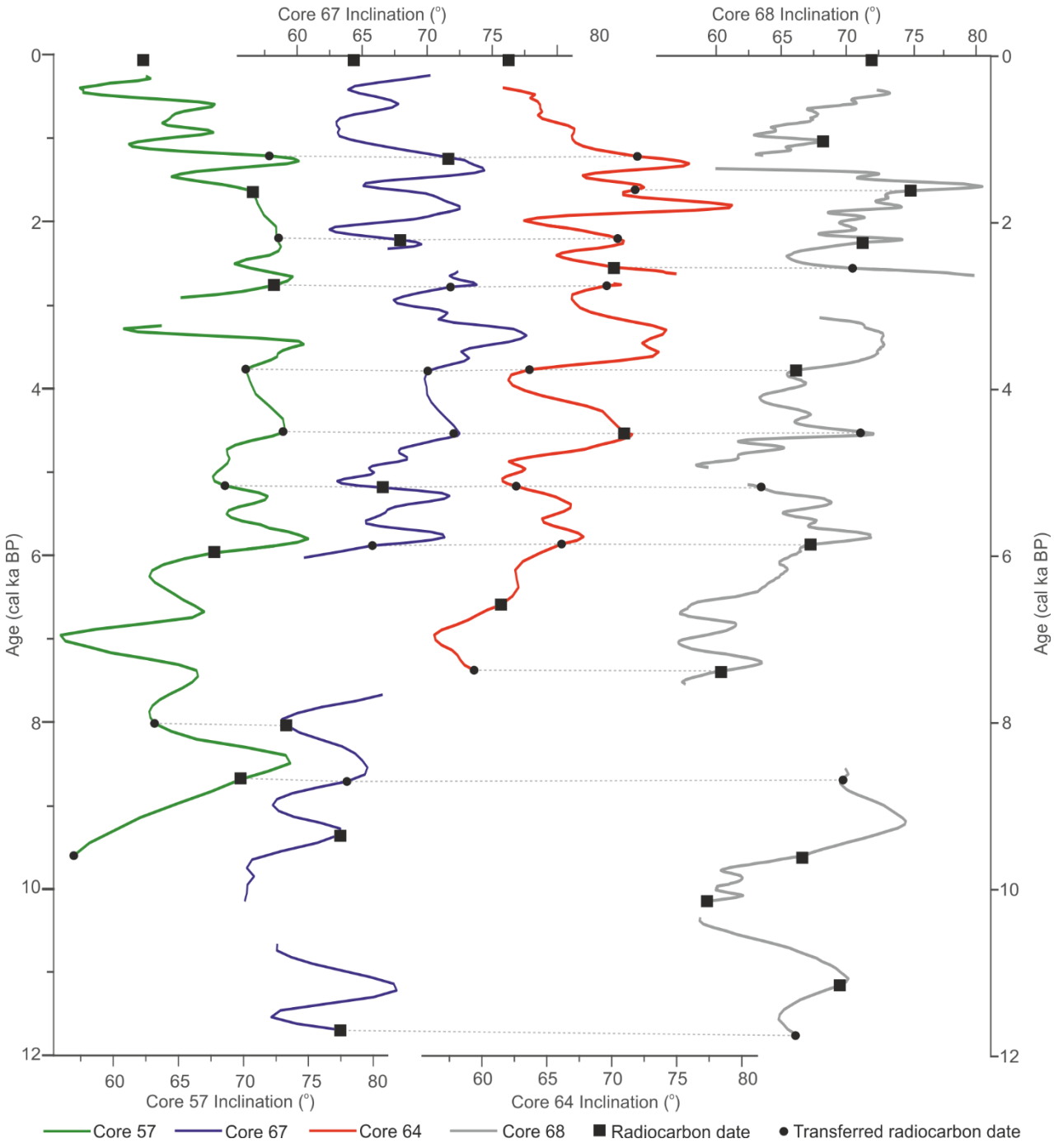

766

767 **Fig. 6**

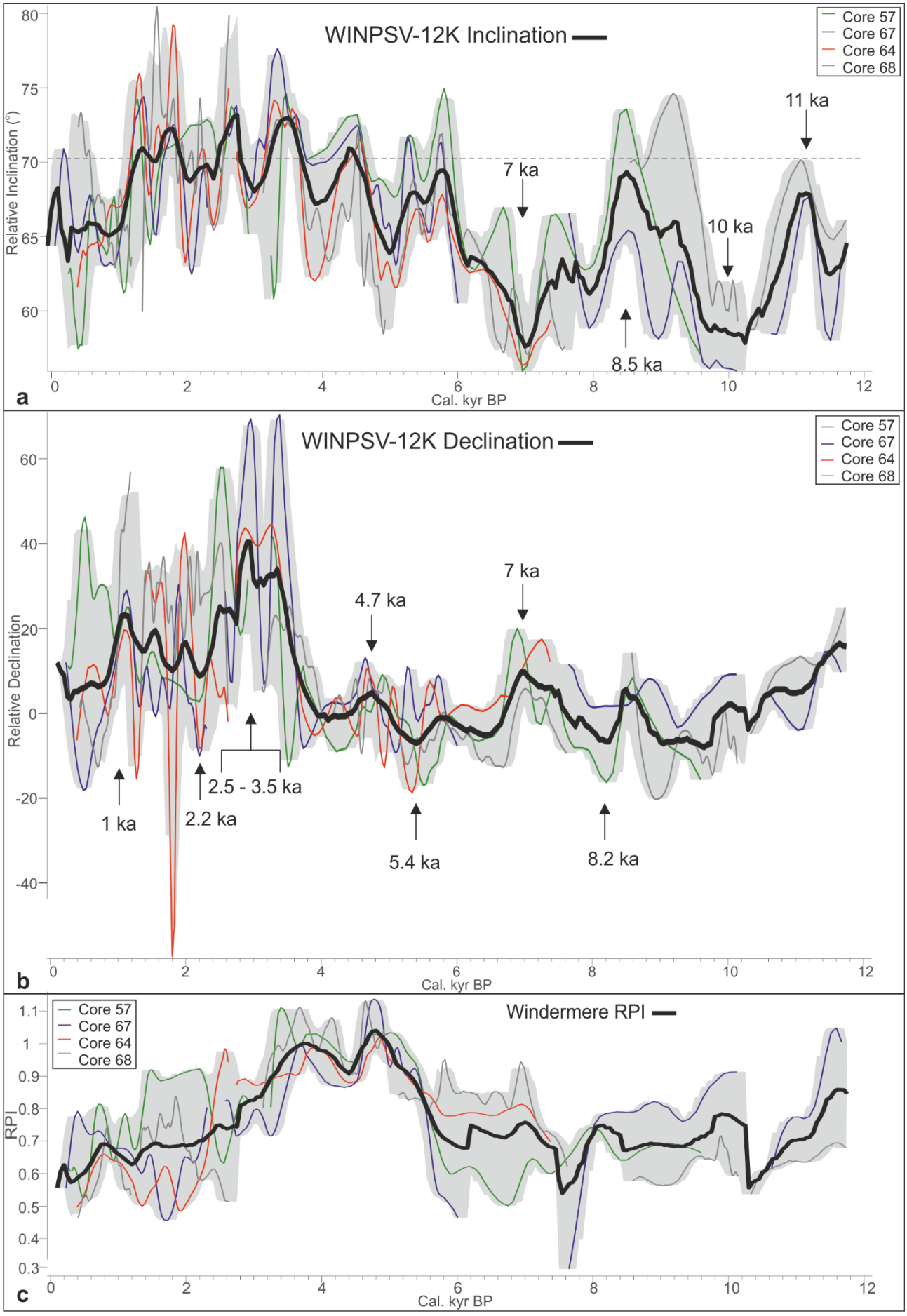
WINPSV-12K Inclination
Core 57
Core 67
Core 64
Core 68
Relative Inclination (°)
11 ka
7 ka
10 ka
8.5 ka
Cal. kyr BP
a
WINPSV-12K Declination
Relative Declination
4.7 ka
7 ka
1 ka
2.2 ka
2.5 - 3.5 ka
5.4 ka
8.2 ka
b
Windermere RPI
RPI
c

768

769 **Fig. 7** (Above)

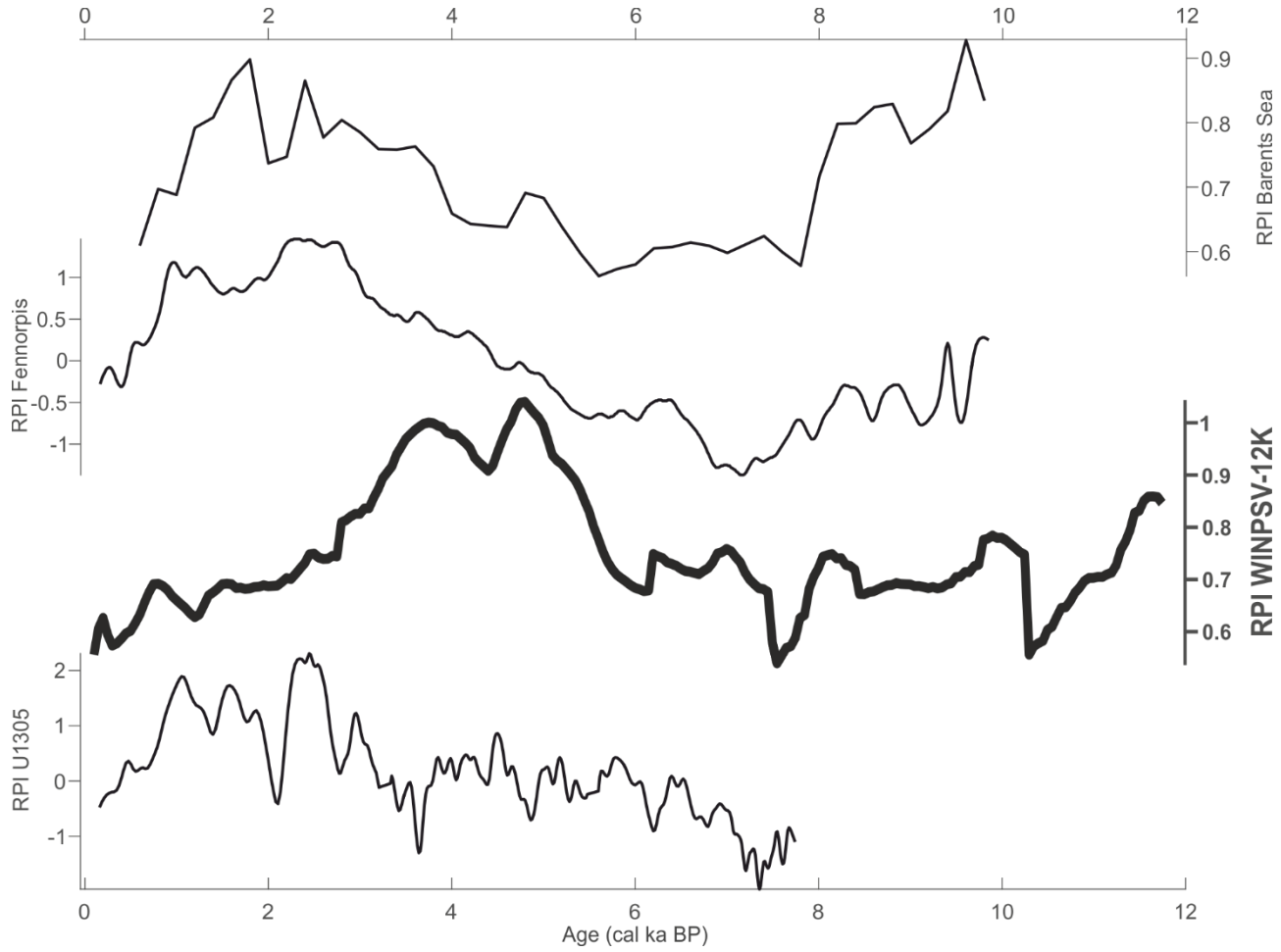

770

771 **Above: Figure 8**

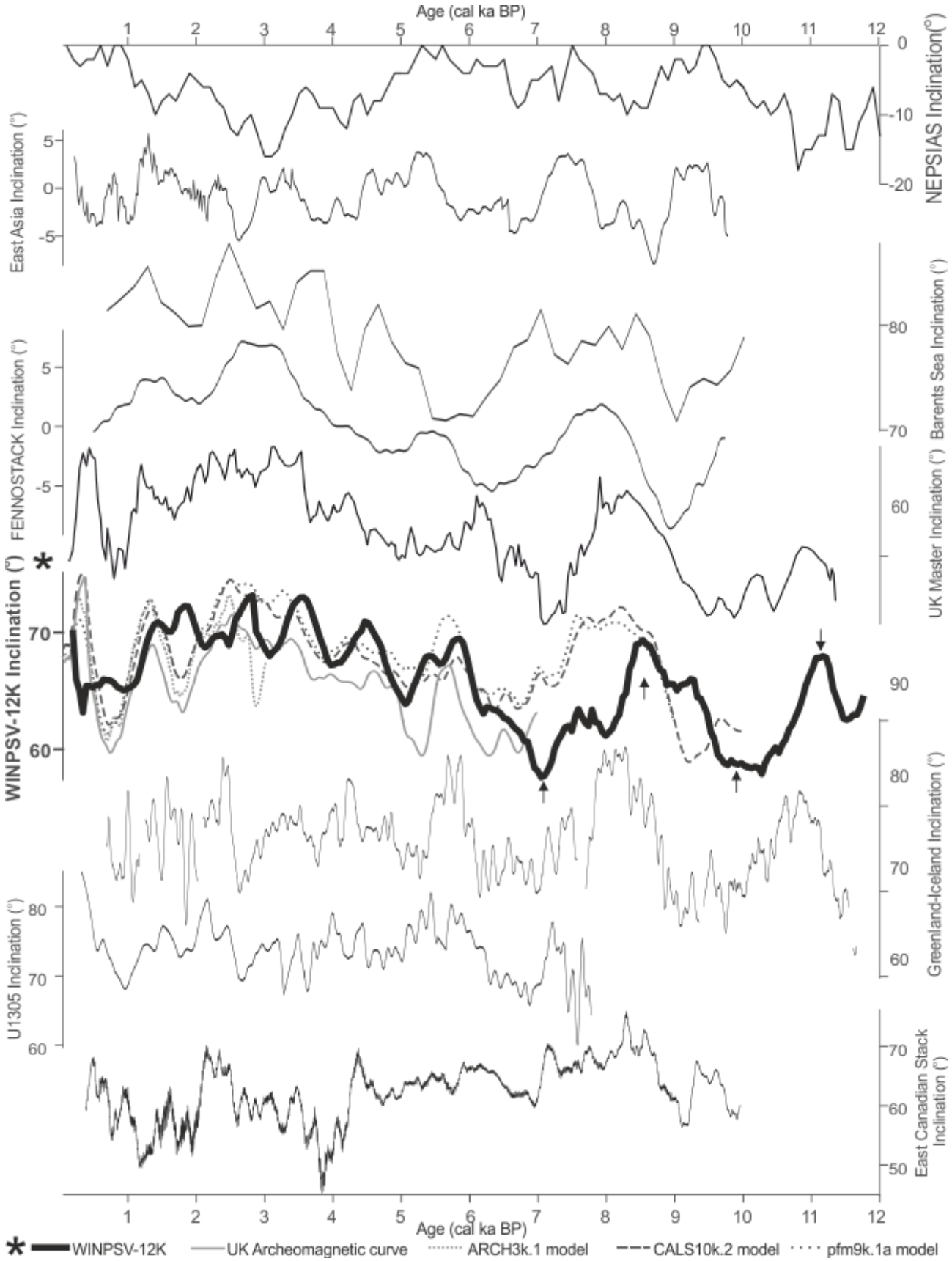
Age (cal ka BP)
NEPSIAS Inclination(°)
East Asia Inclination (°)
FENNOSTACK Inclination (°)
Barents Sea Inclination (°)
UK Master Inclination (°)
WINPSV-12K Inclination (°)
Greenland-Iceland Inclination (°)
U1305 Inclination (°)
East Canadian Stack Inclination (°)
Age (cal ka BP)
WINPSV-12K
UK Archeomagnetic curve
ARCH3k.1 model
CALS10k.2 model
pfm9k.1a model

772

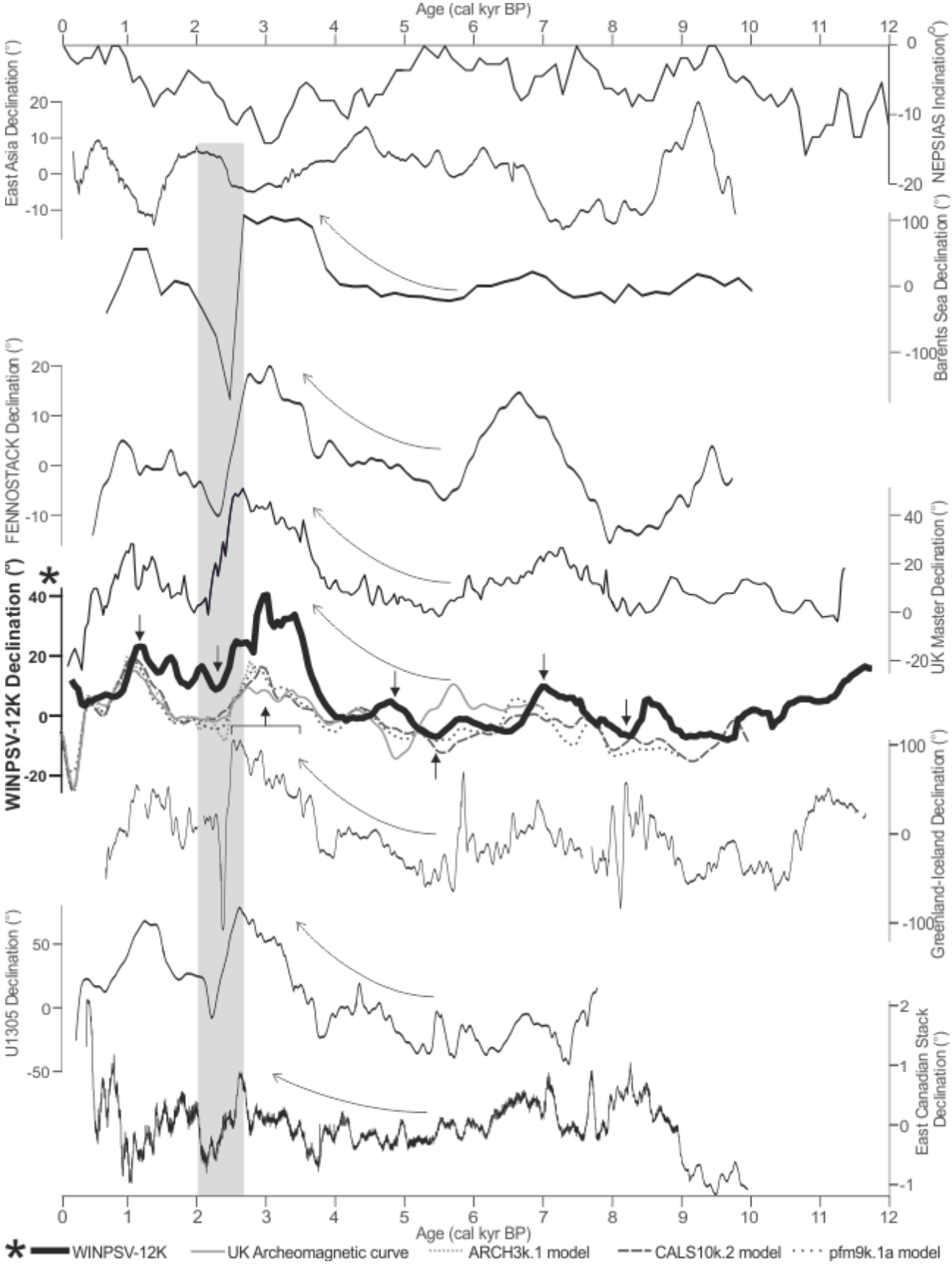
Age (cal kyr BP)
East Asia Declination (°)
NEPSIAS Inclination(°)
Barents Sea Declination (°)
FENNOSTACK Declination (°)
UK Master Declination (°)
WINPSV-12K Declination (°)
Greenland-Iceland Declination (°)
U1305 Declination (°)
East Canadian Stack Declination (°)
WINPSV-12K
UK Archeomagnetic curve
ARCH3k.1 model
CALS10k.2 model
pfm9k.1a model

773

Figs. 9 & 10

SUPPLEMENTARY MATERIAL FOR ONLINE PUBLICATION ONLY

Supplementary Fig. captions

Supplementary Fig. 1. Downcore paleomagnetic records for cores (a) 57, (b) 67, (c) 64, and (d) 68. From left to right, records show: Declination, inclination, maximum angular deviation (MAD), NRM intensity, intensity of progressively acquired anhysteretic remanent magnetization (ARMacq), intensity of progressively demagnetized ARM, ARM/magnetic susceptibility, median destruction field (MDF) of NRM, MDF of ARM, RPI derived from slopes of NRM vs ARMacq, and NRM vs ARM best-fit lines.

Supplementary Fig. 2.

Representative NRM AF demagnetization behaviors of pre-Holocene sediment from Cores 57, 67, 64, and 68. For each selected 1-cm interval from the four cores, the NRM intensity versus AF demagnetization step plot are shown on the left and the orthogonal projection plot of NRM is shown on the right (blue squares = horizontal projections, red circles = vertical projections). Three examples are shown from each core.

Supplementary Fig. 3.

RPI plotted against RPI normalizer (ARMacq) for (a) Core 57, (b) Core 67, (c) Core 64, and (d) Core 68. Numbers indicate R-values of correlation, and the color of the number indicates reliability (red = P-value < 0.05; black = P-value $\geq$ 0.05). The inset in panel (c) indicates the correlation between RPI and ARMacq for Core 64 prior to 2 cal ka BP.

Supplementary Fig. 4

Supplementary Figure xx. Virtual geomagnetic pole (VGP) positions estimated from WINPSV-12K (red circles), East Asia PSV stack (Zheng et al., 2014) (black circles), and Barents Sea PSV record (Sagnotti et al., 2012) (yellow circles). See Figure 1a for record locations. Overlaid contour map shows the vertical component of magnetic field at the core-mantle boundary averaged over the 1590-1840 time interval (after Gubbins et al., 2006; Stoner et al., 2013).

Supplementary Tables

Supplementary Table 1. NRM and ARM demagnetization treatment steps and measurement resolution for U-channel samples from Cores 57, 67, 64 and 68.

Measurement interval, cm	Alternating field demagnetization step peak field, , mT	No. steps
0.5	0, 5, 10, 15, 20, 25, 30, 35, 40, 45, 50, 55, 60, 70, 80, 90, 100	17
1	0, 10, 20, 25, 30, 35, 40, 45, 50, 55, 60, 65, 70, 80, 90, 100	16
1	0, 10, 20, 25, 30, 35, 40, 45, 50, 55, 60, 65, 70, 80, 90, 100	16
1	0, 10, 20, 25, 30, 35, 40, 45, 50, 55, 60, 65, 70, 80, 90, 100	16

Supplementary Table 2. Accelerator Mass Spectrometry Radiocarbon measurements and subsequent calibrated radiocarbon ages in calendar years BP for Cores 57, 67, 64 and 68

Core	Depth, cm	Sample number	Material dated	Weight, mg	Reported age, 14C y BP	Median Probability, cal y BP	Min. 2σ	Max. 2σ
57[a]	19.4	-	Bulk	-	33	-	-	-
57	72.3	SUERC-64862	Wood	-	1739	1651	1554	1732
57	86.0	SUERC-62199	Leaf	90	2646	2765	2737	2844
57	143.6	SUERC-62194	Bulk	11000	5227	5974	5912	6175
57	176.6	SUERC-62208	Bulk	5120	7885	8688	8588	8972
67[a]	21.1	-	Bulk	58	-	-	-	-
67	48.1	SUERC-62198	Twig	20	1260	1214	1083	1282
67	80.2	SUERC-52714	Leaf	-	2181	2199	2068	2315
67	160.4	SUERC-55686	Leaf	-	4505	5168	5044	5301
67	211.2	SUERC-55684	Leaf	-	7209	8018	7955	8157
67	228.5	SUERC-55685	Seed	-	8302	9324	9140	9434
67	257.2	SUERC-62213	Bulk	10360	10119	11750	11409	12003
64[a]	17.6	-	Bulk	60	-	-	-	-
64	85.0	SUERC-62194	Leaf	230	2456	2544	2363	2705
64	129.4	SUERC-62203	Leaf	70	4046	4519	4423	4784
64	170.1	SUERC-62204	Bulk	10300	5790	6591	6491	6673
64	219.2	SUERC-62209	Bulk	13100	10008	11489	11280	11709
68[a]	14.5	-	Bulk	-	-13	-	-	-
68	72.0	SUERC-64854	Bulk	-	1114	1020	934	1172
68	120.7	SUERC-64859	Bulk	-	1708	1614	1548	1702
68	171.4	SUERC-52708	Leaf	-	2242	2232	2153	2342
68	237.7	SUERC-52709	Leaf	-	3499	3771	3649	3866
68	329	SUERC-52710	Leaf	-	5124	5862	5748	5939
68	377.1	SUERC-62207	Bulk	10600	6468	7375	7295	7439
68	428.2	SUERC-52711	Leaf	-	8653	9600	9539	9688
68	454.4	SUERC-62206	Bulk	11900	9061	10225	10180	10260
68	521.7	SUERC-52713	Twig	-	9708	11160	10881	11225

[a] Calendar age ascertained using ^{137}Cs and ^{210}Pb radiochronology

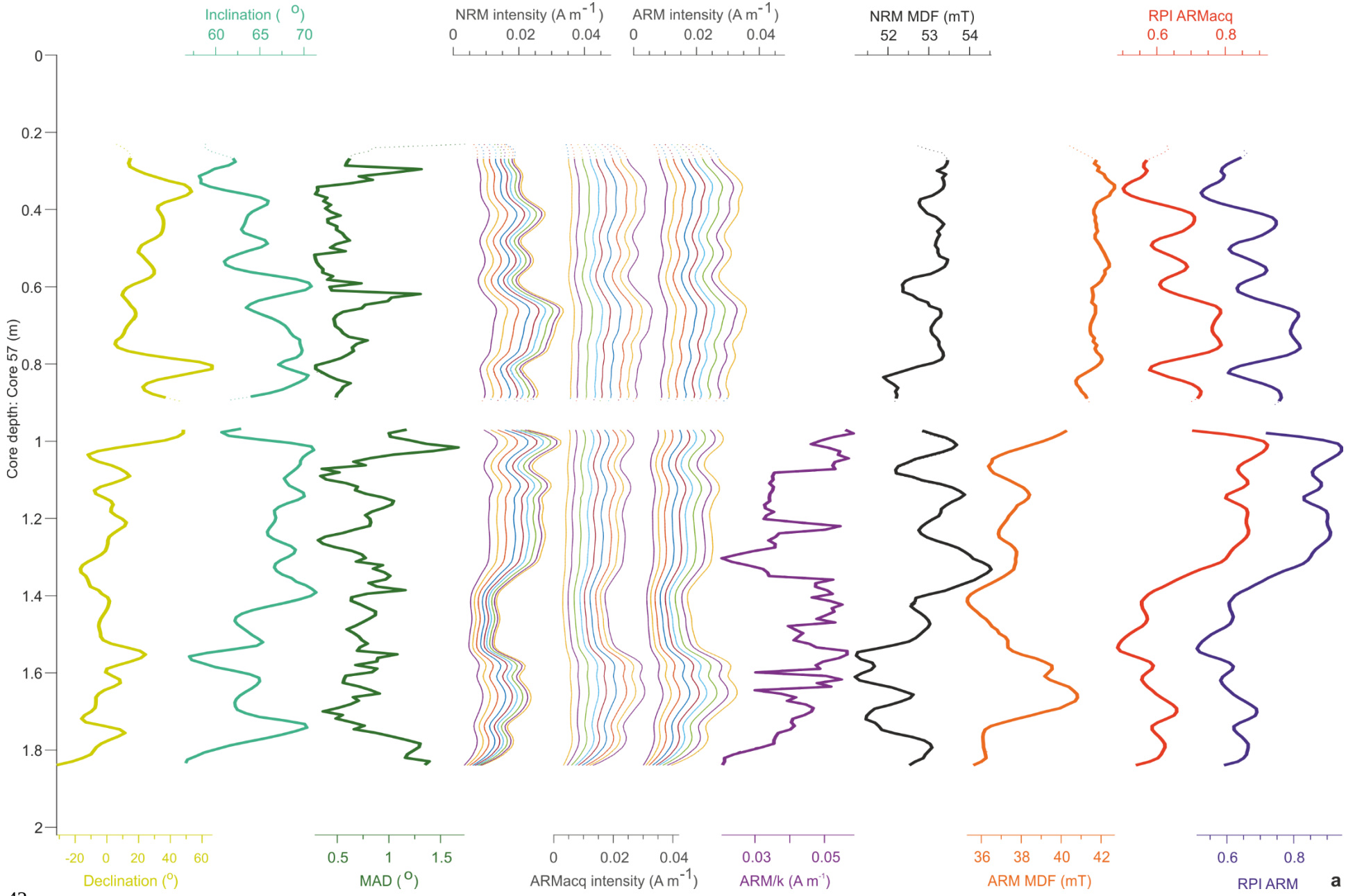
Inclination (o)
60 65 70
NRM intensity (A m-1)
0 0.02 0.04
ARM intensity (A m-1)
0 0.02 0.04
NRM MDF (mT)
52 53 54
RPI ARMacq
0.6 0.8
Core depth: Core 57 (m)
0
0.2
0.4
0.6
0.8
1
1.2
1.4
1.6
1.8
2
-20 0 20 40 60
Declination (o)
0.5 1 1.5
MAD (o)
0 0.02 0.04
ARMacq intensity (A m-1)
0.03 0.05
ARM/k (A m-1)
36 38 40 42
ARM MDF (mT)
0.6 0.8
RPI ARM
a

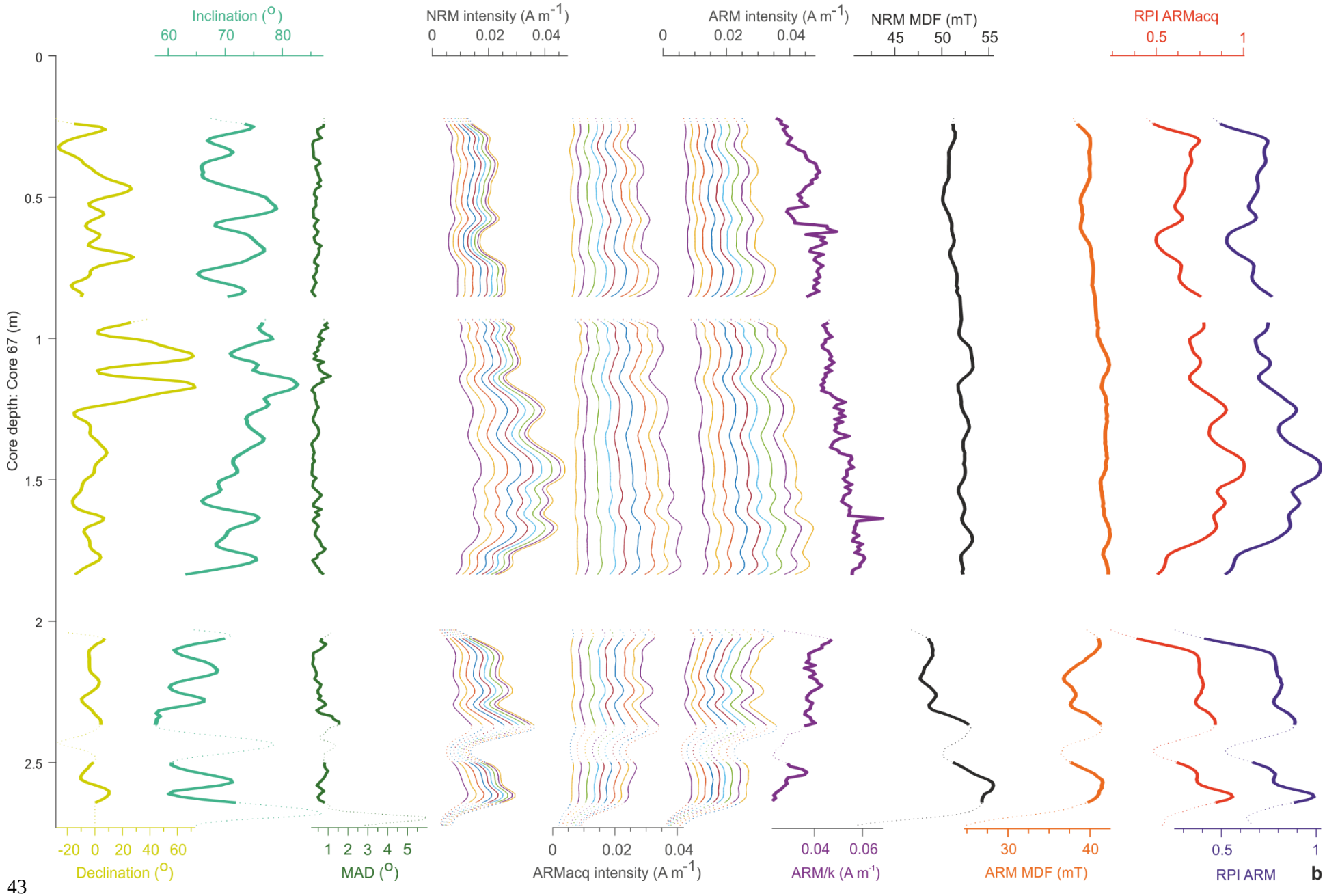
Inclination (°)
60 70 80
NRM intensity (A m-1)
0 0.02 0.04
ARM intensity (A m-1)
0 0.02 0.04
NRM MDF (mT)
45 50 55
RPI ARMacq
0.5 1
Core depth: Core 67 (m)
0
0.5
1
1.5
2
2.5
-20 0 20 40 60
Declination (°)
1 2 3 4 5
MAD (°)
0 0.02 0.04
ARMacq intensity (A m-1)
0.04 0.06
ARM/k (A m-1)
30 40
ARM MDF (mT)
0.5 1
RPI ARM
b

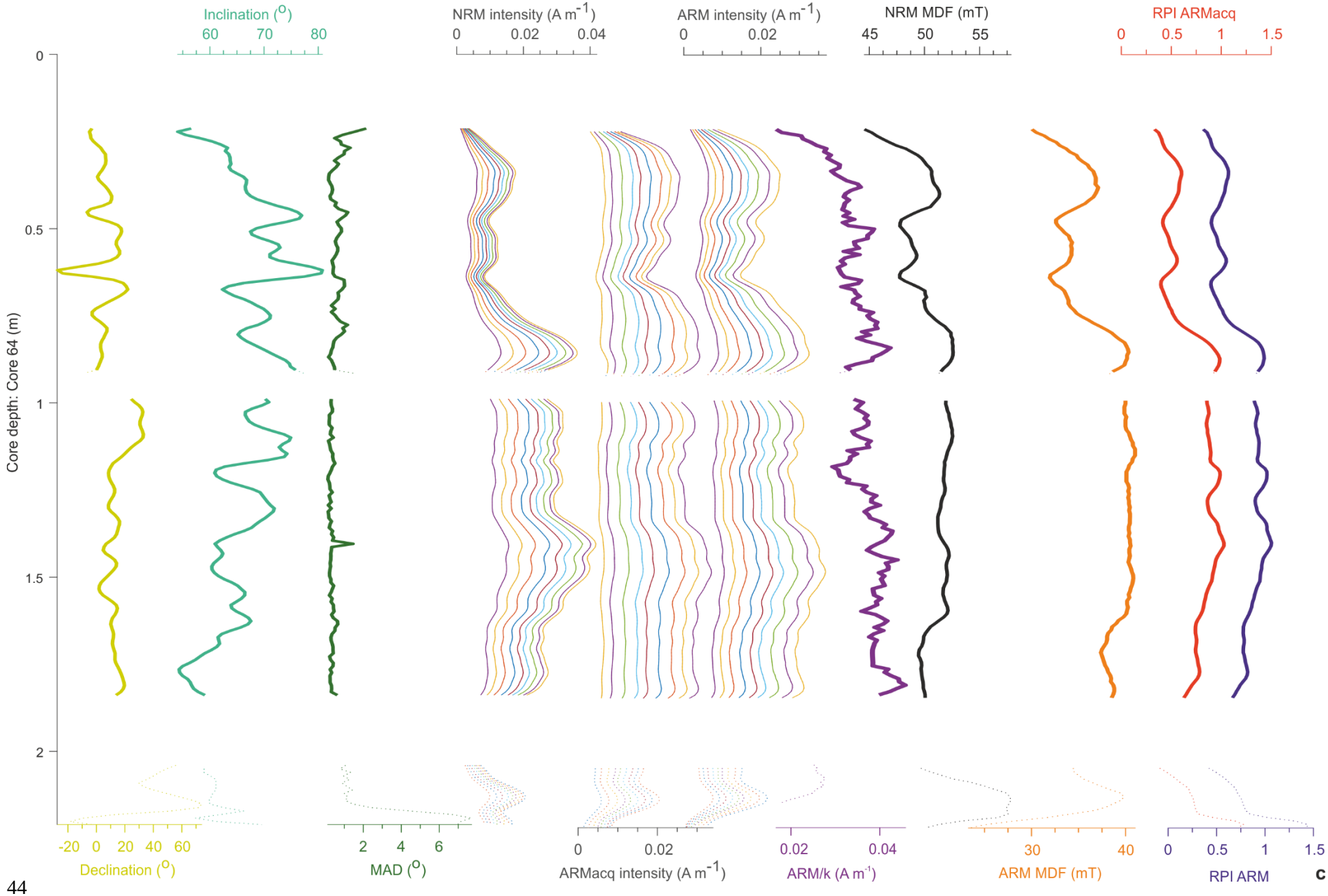
Inclination (°)
60 70 80
NRM intensity (A m-1)
0 0.02 0.04
ARM intensity (A m-1)
0 0.02
NRM MDF (mT)
45 50 55
RPI ARMacq
0 0.5 1 1.5
Core depth: Core 64 (m)
0
0.5
1
1.5
2
-20 0 20 40 60
Declination (°)
2 4 6
MAD (°)
0 0.02
ARMacq intensity (A m-1)
0.02 0.04
ARM/k (A m-1)
30 40
ARM MDF (mT)
0 0.5 1 1.5
RPI ARM
c

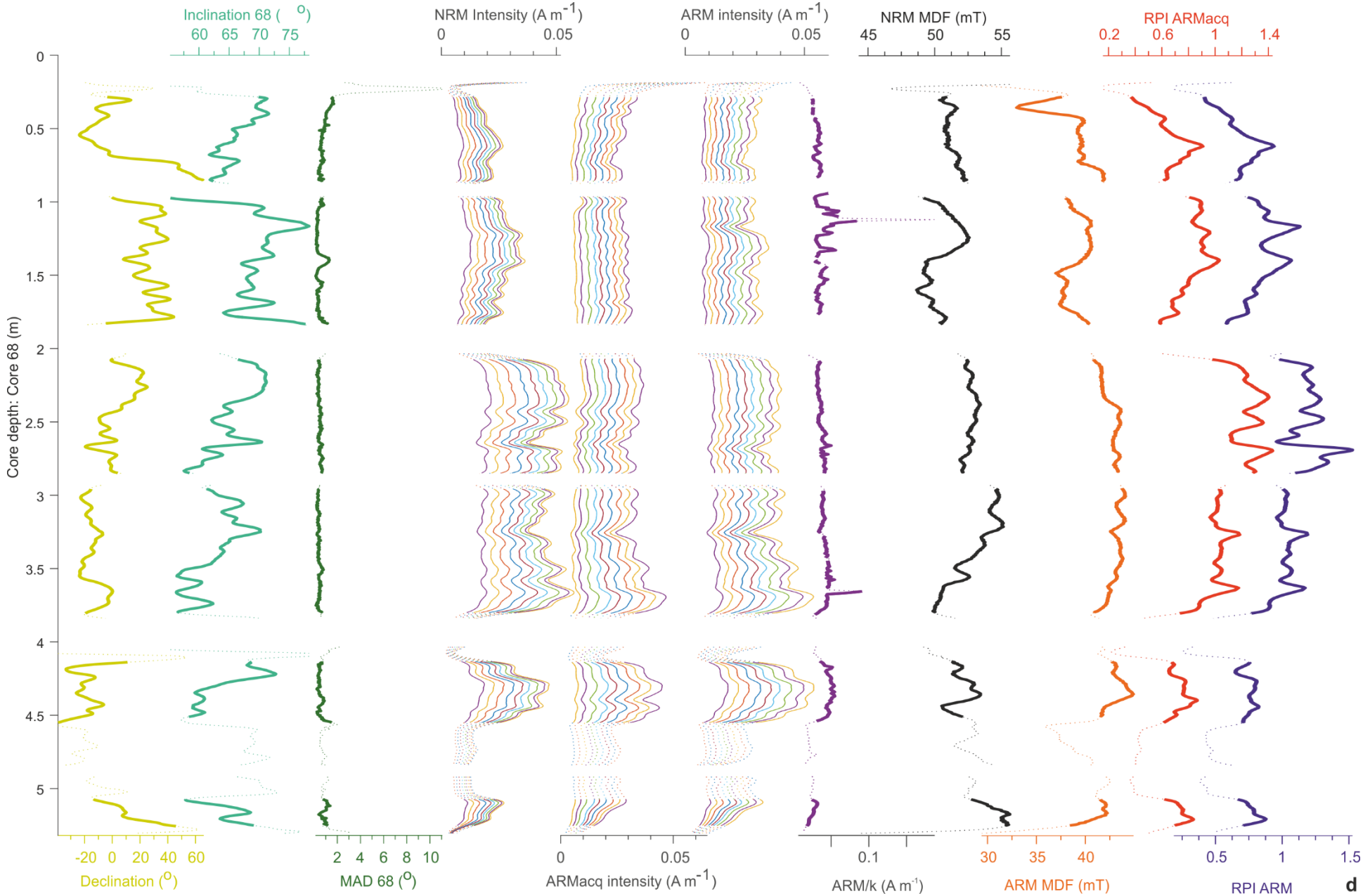
Inclination 68 (O)
60 65 70 75
NRM Intensity (A m-1)
0 0.05
ARM intensity (A m-1)
0 0.05
NRM MDF (mT)
45 50 55
RPI ARMacq
0.2 0.6 1 1.4
Core depth: Core 68 (m)
0 0.5 1 1.5 2 2.5 3 3.5 4 4.5 5
-20 0 20 40 60
Declination (O)
2 4 6 8 10
MAD 68 (O)
0 0.05
ARMacq intensity (A m-1)
0.1
ARM/k (A m-1)
30 35 40
ARM MDF (mT)
0.5 1 1.5
RPI ARM
d

Supp. Fig. 1

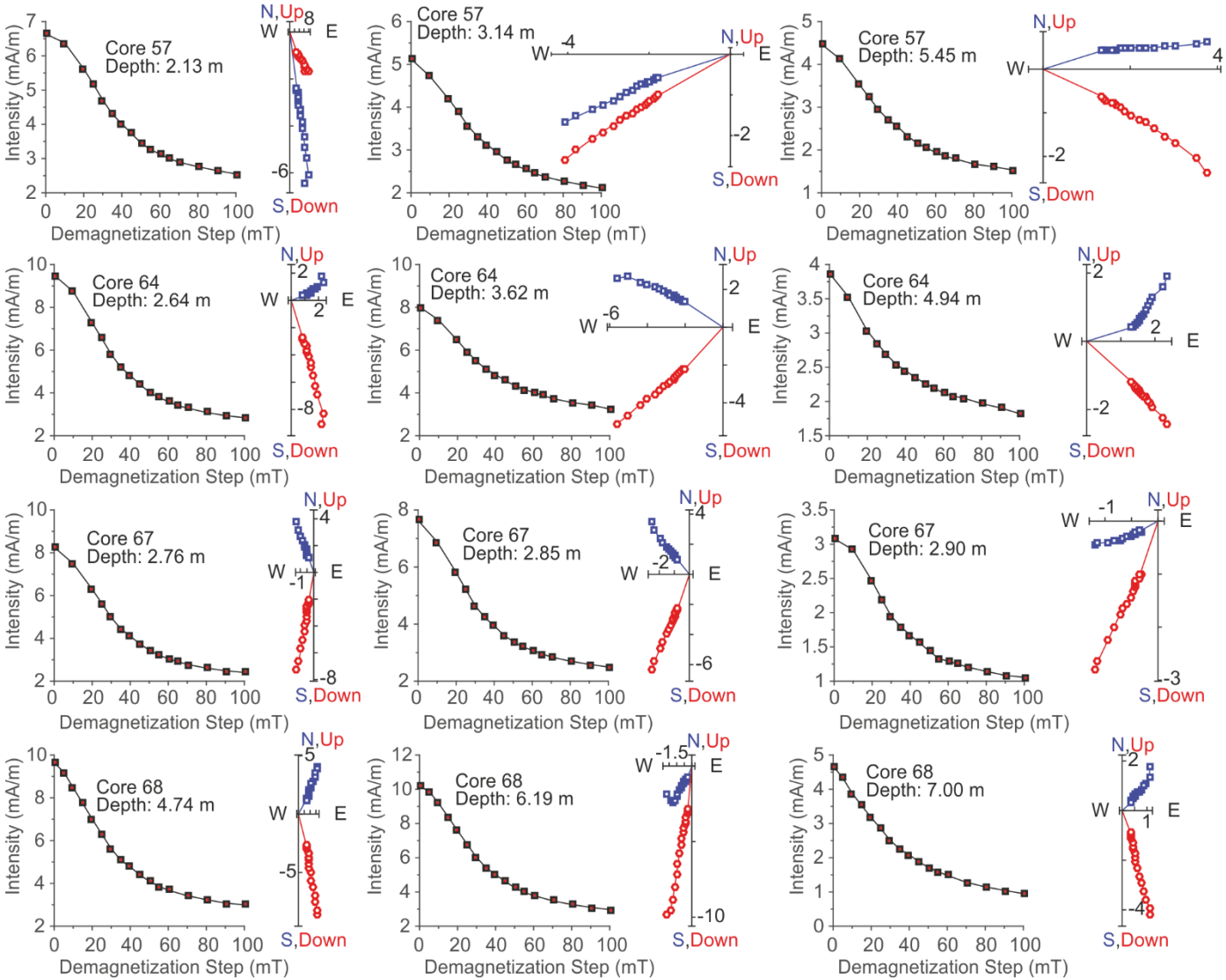

821

822 Supp. Fig. 2

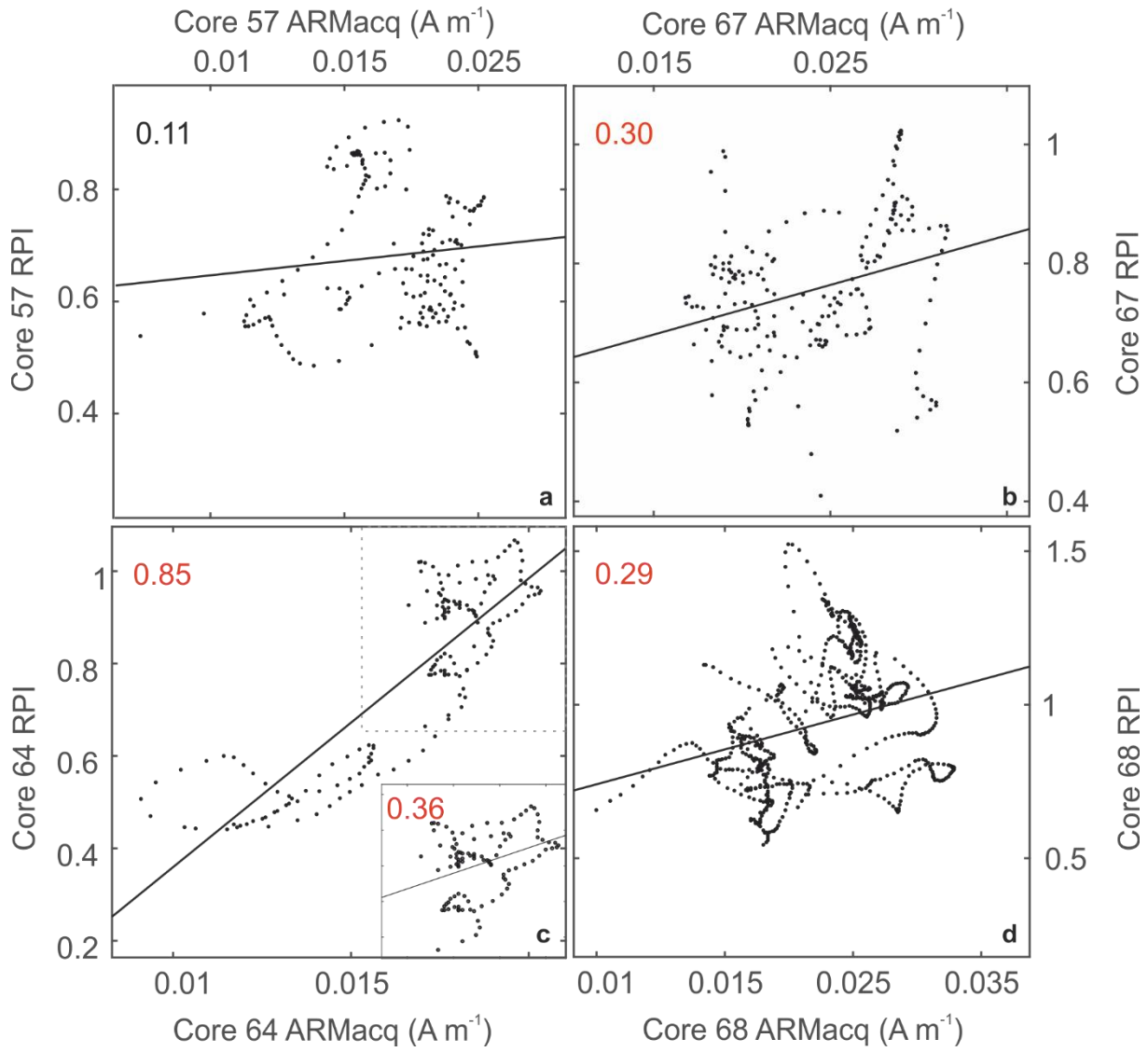

823

824 Supp. Fig. 3

825

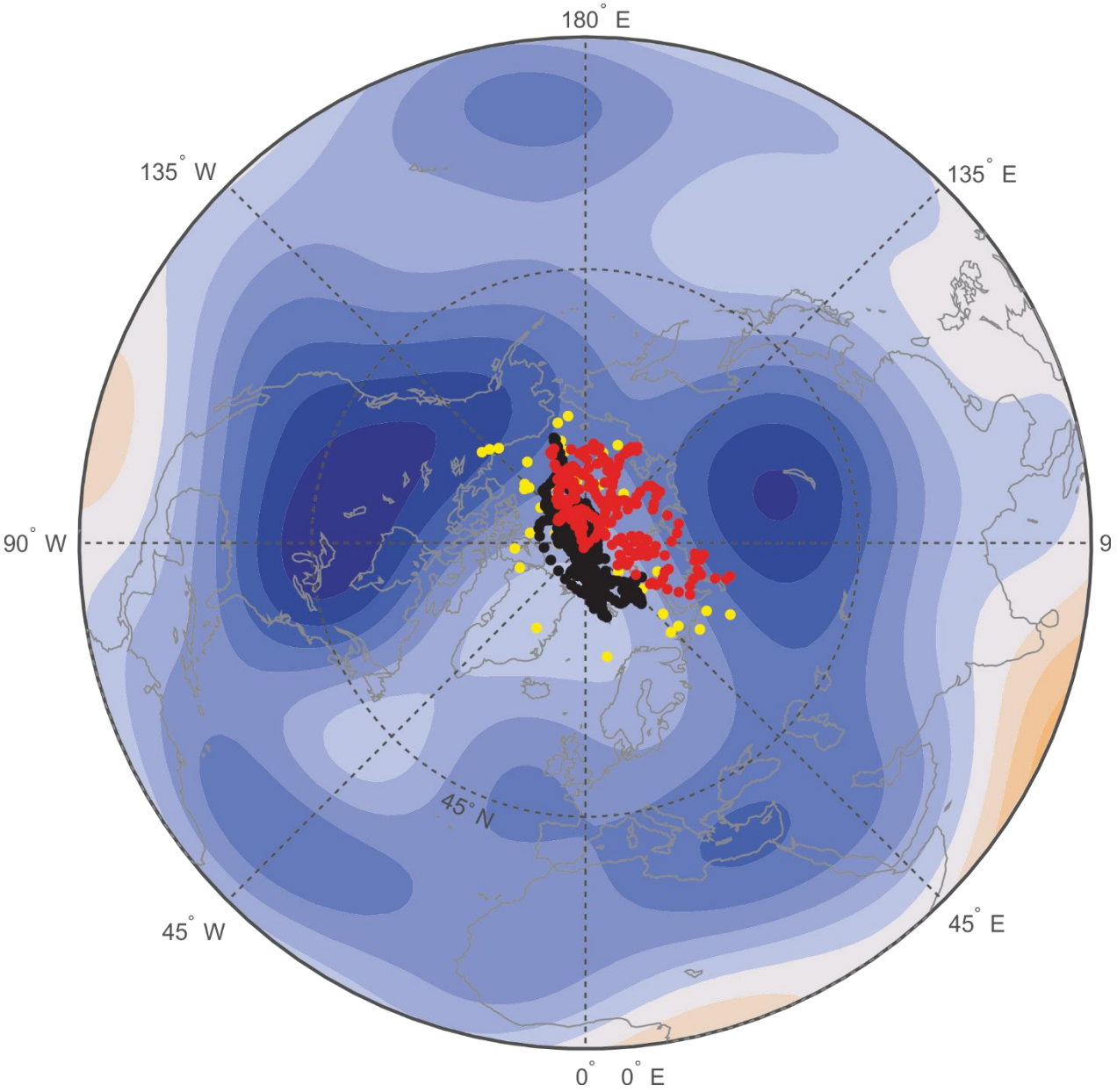

826

827 Supp. Fig. 4

828 **Additional citation used only in Supplementary Fig. 4:**

829 Gubbins, D., Jones A. L., Finlay C. C., 2006. Fall in Earth's magnetic field is erratic. Science, 312, 900–902.

830